

ADAPTIVE FORCE CONTROL IN COMPLIANT MOTION

Homayoun Seraji

Jet 1 'repulsion Laboratory
California Institute of Technology
Pasadena, CA 91109

Abstract

This paper addresses the problem of controlling a manipulator in compliant motion while in contact with an environment having an unknown stiffness. Two classes of solutions are discussed: *adaptive admittance control* and *adaptive compliance control*. Admittance control is an *explicit* force control scheme in which a force setpoint is specified and is tracked by the force compensator. Two adaptive PID and PI force compensators are proposed in the paper which ensure *robust* tracking of step setpoints and rejection of constant disturbances. Compliance control, on the other hand, is an *implicit* force control scheme and establishes a user-specified target interaction dynamics between the reference position and the contact force. Two adaptive lag-plus-feedforward compliance compensators are developed in the paper. The PI force compensator and the proposed compliance compensators do *not* require force rate information for implementation. In both admittance and compliance control schemes, since the environmental stiffness can typically vary by several orders of magnitude, compensator adaptation is used to ensure a stable and uniform system performance. Dynamic simulation results for a 7 DOF Robotics Research arm are presented to demonstrate the efficacy of the proposed control schemes in executing contact tasks.

1 introduction

Robust and reliable operation of manipulators in contact with objects in their environment is the basic requirement for successful execution of many robotic tasks. Stable control of robot-environment interaction poses a technically challenging problem, and has attracted the attention of several roboticists for almost two decades. In 1977, Whitney [1] proposed a simple scheme for contact control called "(position accommodation" where the contact force is used to modify the reference position trajectory. In 1981, Raibert and Craig [2] suggested the "hybrid control" approach where certain Cartesian directions are under position control while the others are under force control. In a seminal paper in 1985, Hogan [3] proposed "impedance control" which attempts to establish a user-specified dynamic relationship between the end-effector position and force. Compliant motion control, which is in essence position-based force control, has been suggested by Kazerooni [4-9] and Lawrence [10-13] in a series of papers. Several other researchers have also contributed to the deeper understanding and further development of contact control schemes, such as [14-41] to name a few.

The objective of this paper is to develop two simple and pragmatic approaches to contact force control using the compliant motion framework. The first proposed approach, called *adaptive admittance control*, is an *explicit* force control scheme which ensures robust force setpoint tracking with desirable dynamic response. This approach is based on the concept of mechanical admittance, which relates the contact force to the resulting velocity perturbation. The second proposed approach, called *adaptive compliance control*, is an *implicit* force control scheme in which the reference position is used as a command to control the contact force, and no force setpoints are used. Two simple adaptive compliance compensators are developed which possess enhanced stability and improved performance over the conventional compliance compensator. In both the admittance and compliance control approaches, compensator adaptation is used to provide stable and uniform performance under gross variation of the environmental stiffness.

The paper is structured as follows. Section 2 discusses force control within the compliant motion framework. The concept of virtual forces for proximity control is discussed in Section 3. Two adaptive admittance control schemes resulting in PID and PI force compensators are discussed in Section 4 to ensure force setpoint tracking. In Section 5, adaptive lag-plus-feedforward compensators are developed to accomplish compliance with the environment. In Section 6, the Robotics Research arm is used in a series of dynamic simulations to demonstrate force and compliance control. The paper is concluded in Section 7 with a review and general discussions.

2 Force Control in Compliant Motion

Robot manipulators are always supplied with joint servo controllers which ensure tracking of joint setpoints, and, in turn, enable the placement and orientation of their end-effectors in the workspace. For unconstrained free-space motions, the end-effector Cartesian coordinates

X (typically, a 6×1 vector of position and orientation) can follow a user-specified nominal or reference motion trajectory X_r using the joint servos and inverse kinematic transformation. The underlying concept of compliant motion control is to use the position-controlled robot as a baseline system and to make the necessary modifications to this system to enable execution of constrained tasks that require robot interaction with the environment. Figures 1 and 2 show the block diagrams of position-based explicit and implicit force control systems (including the force setpoint F_r) when the robot interacts with the environment. The force/torque sensor mounted on the end-effector detects this interaction and measures the contact force F . This sensory data is then fed back and used in real-time to modify or perturb the reference motion trajectory X_r to assure a desirable behavior of manipulator-environment interaction. This is accomplished by commanding the end-effector to deviate by the amount X_f from its reference trajectory and track the modified commanded trajectory X_c . The perturbation X_f is generated by the force or compliance compensator which modifies the nominal end-effector motion automatically in response to the force/torque sensory data in order to attain the required interaction characteristics. In general, the compensator is not restricted to have an algebraic-differential model and can perform logical operations or follow certain rule-based decisions. The manipulator can also be driven from a multitude of other external sensors, and the compensator can perform sensor fusion and make the necessary trajectory modification based on multiple sensory data.

Now, since the manipulator position control system ensures Cartesian trajectory tracking, the position controller, in effect, causes each end-effector coordinate to track the corresponding command and to reject the disturbances caused by other commands. As a result, we can consider each end-effector coordinate independently and replace the end-effector position vector X in the control diagram by the scalar x , which can represent *any* element of X . Furthermore, following Kazerooni [7], Lawrence [10], and other researchers, it is reasonable to model each position-controlled end-effector coordinate by a second-order linear continuous-time system, so that for each end-effector coordinate the scalar transfer-function relating the commanded position x_c to the actual position x is given by

$$G(s) = \frac{x(s)}{x_c(s)} = \frac{K_m}{J_m s^2 + B_m s + K_m} = \frac{b}{s^2 + as + b} \quad (1)$$

where J_m , B_m , and K_m are the position-control manipulator mass, damping and stiffness parameters in Cartesian-space, respectively, and $a = \frac{B_m}{J_m}$ and $b = \frac{K_m}{J_m}$. This simple model can adequately account for the small time-delays involved in the forward and inverse kinematic calculations as well as the dynamics of the position-controlled joint servo loops. This model is particularly suitable for industrial robots that use high gear ratios which attenuate the nonlinear manipulator dynamics and make the second-order joint motor dynamics dominant [42].

The environment can often be modeled as a linear spring with coefficient of stiffness K_{en} along the Cartesian axis of interest. Therefore, the force-displacement model for the environment is given by Hooke's law as

$$F' = K_{en}(x - x_e) \quad (2)$$

where x_e is the nominal position of the environment. Similarly, the force/torque sensor mounted on the end-effector can be modeled as a pure spring with the stiffness coefficient K_{sn} , since the dynamics of the sensor can be neglected in comparison with the compensator and manipulator time-constants. Therefore, the effective stiffness of the sensor plus the environment in a Cartesian direction is given by $K_e = (1/K_{en} + 1/K_{sn})^{-1}$. Note that although the manipulator-environment interaction can be modeled in detail as a high-order dynamical system [36, 38], the stiffness is often the dominating factor in contact tasks such as assembly, mating, and deburring [10, 19, 35]. Furthermore, this simple model is mathematically tractable and has been widely adopted by several researchers. It is important to note that when the robot is in contact with the environment, the dynamic model of the position-controlled end-effector coordinate is modified by the environment due to natural force feedback as

$$J_m \ddot{x} + B_m \dot{x} + K_m x = K_m x_c - K_e x \quad (3)$$

since the contact force $K_e x$ will now oppose the motion into the environment. Hence, at contact, the modified transfer-function $\tilde{G}(s)$ takes the form

$$\tilde{G}(s) = \frac{x(s)}{x_c(s)} = \frac{K_m}{J_m s^2 + B_m s + (K_m + K_{en})} = \frac{b}{s^2 + as + b'} \quad (4)$$

where $b' = \frac{K_m + K_e}{J_m}$. Note that the feedback loop $K_e x$ closes naturally as the robot encounters the environment.

In this paper, we present two different approaches to force control: *admittance control* and *compliance control*. In the admittance control scheme discussed in Section 4, the reference position x_r is a constant exogenous input used to ensure that the end-effector is initially in contact with the environment. Force control, however, is accomplished by applying the force setpoint F'_r as a command input to control the contact force F' as the output. In the compliance control scheme addressed in Section 5, the reference position x_r is used as a command input to control the contact force F' , and no force setpoint is applied ($F'_r = 0$). In compliance control, x_r is chosen to "penetrate" into the environment by an appropriate amount in order to produce the desired contact force. Therefore, to accomplish a constant contact force, the reference motion trajectory x_r is specified as a constant during constrained motion. In the absence of the force feedback perturbation x_f , the steady-state contact force F'_x solely due to the constant reference motion trajectory x_r is obtained from Figure 2 as

$$F'_x = k_e \left[\frac{b}{b'} x_r - x_e \right] \quad (5)$$

When the environmental parameters (k_e, x_e) and the robot parameters (b, b') are known *precisely*, the reference trajectory x_r can be computed from (5) to produce the desired contact

force $F_x = F_r$. In practice, however, this "open-loop" approach to force control which requires exact knowledge of the system parameters (k_e, x_e, b, b') is unacceptable, and "closed-loop" approach employing force feedback is desirable since it does not require knowledge of the system parameters.

Before addressing admittance and compliance control, we show that the compliant motion control framework can also be used to accomplish "(proximity control)" based on virtual forces generated by proximity sensors or dynamic world models.

3 Proximity Control using Virtual Forces

In Section 2, the robot end-effector makes physical contact with the environment and "real" forces and torques are generated based on this contact, in this section, the concepts laid out in Section 2 will be used for "virtual" forces and torques in order to accomplish proximity control relative to the environment [25, 34, 36].

Virtual forces and torques can be generated based on the end-effector proximity to the environment using either proximity sensors or dynamic world models as discussed below.

3.1 Proximity Sensors

These sensors produce an output in response to the distance from an object. There is a wide variety of commercial proximity sensors with different ranges of operation and physical principles. Figure 3 shows the characteristic of a typical in-proximity sensor using the infra-red triangulation method. The sensor produces a current output, ranging from $4mA$ to $20mA$ in response to the object distance in the range of $520mm$ to $180mm$. The current output can be converted to a voltage output ranging from $1V$ to $5V$ by connecting a resistor across the output. In the linear operating range AB shown in Figure 3, the sensor can be modeled as

$$F_s = F_0 + k_s \cdot [d_0 - d_s] \quad (6)$$

where d_s is the sensed distance-to-object in mm , $d_0 = 520mm$, k_s is the slope of the sensor characteristic ($= \frac{20A - 4A}{520 - 180} = 0.047mA/mm$), F_s is the sensor current output in mA , and $F_0 = 4772A$. Equation (6) can be interpreted as the force-displacement relationship for a "(virtual" spring with stiffness k_s . Therefore, the proximity sensor output can be used to perturb the nominal motion trajectory x_r based on the virtual force F_s , as discussed in Section 2.

3.2 Dynamic World Models

in an analogous manner to proximity sensing, world model information can be used to generate "fictitious" forces based on distances to objects in the geometric database of the robot workspace. For instance, suppose that there is a moving object in the robot workspace. A vision system can detect the position of the object and attach a fictitious surface to the object in the world model. The robot then reacts to this surface by experiencing a "fictitious" force

F_w that reflects proximity to the surface. The force F_w can be generated in the software such that as the end-effector approaches the surface, the magnitude of F_w increases. A simple representation of this behavior is

$$F_w = \begin{cases} k_w [x - c] & \text{for } x > c \\ 0 & \text{for } x \leq c \end{cases} \quad (7)$$

Where x is the end-effector position, c represents the surface location, k_w is the stiffness of the fictitious spring between the end-effector and the surface, and F_w is the fictitious force. Equation (7) generates a force proportional to the end-effector/surface distance. This approach can be used to avoid collision between two robot arms working in a common workspace by attaching a fictitious surface in the software to the end-effector of one robot and continuously updating the geometric world model for the second robot.

The virtual forces generated based on object distance can be used for two purposes:

(i) **Collision Avoidance:** Avoidance of collision with objects in the robot workspace is a basic requirement in all robotic tasks. The collision avoidance requirement can simply be expressed as the inequality

$$F_v < F_T$$

where F_v is the virtual force generated by the proximity sensor or world model, and F_T is some threshold force which reflects the allowable buffer for dynamic collision avoidance. Using the compliant control system described in Section 2, we can form the force tracking-error as

$$e = \begin{cases} 0 & \text{for } F_v \leq F_T \\ F_v - F_T & \text{for } F_v > F_T \end{cases} \quad (8)$$

and use the admittance control approach described in Section 4 to ensure that the nominal motion is perturbed such that e tends to zero.

(ii) **Maintaining a Constant Distance:** For execution of some robotic tasks such as surface inspection or contour following, the robot end-effector must be maintained at a constant distance from a surface. This requirement can simply be expressed as

$$F_v = F_r \quad (9)$$

where F_r reflects the desired distance-to-object. Using the admittance control approach of Section 4, we can ensure that the compliant control system meets this requirement.

Note that in dealing with virtual forces based on proximity sensors or dynamic world models, the rate-of-change of the force signal is readily available in software and can be used in the control law implementation. This is in contrast to the contact force measured by the force/torque sensor which is a noisy signal and cannot be differentiated directly.

4 Adaptive Admittance Control

Let us now consider the explicit force control system shown in Figure 1. The end-effector/environment contact force F is measured by the force/torque sensor and is compared with the desired force setpoint F_r specified by the user. The force compensator $K(s)$ uses the force error information $e = F_r - F$ to generate the necessary trajectory modification x_f on-line and in real-time, and the end-effector then tracks the modified motion trajectory $x_c = x_r + x_f$ as closely as possible. Note that the force setpoint F_r is specified at the instant the robot contacts the environment initially and is reset to zero when the end-effector contact task is terminated, so that during free-space motion $F_r = 0$.

In contrast to pure position control which rejects disturbance forces in order to track a given reference motion trajectory, the force compensator $K(s)$ attempts to "comply" with the environmental interaction and react quickly to contact forces by rapidly modifying the reference motion trajectory. A proper measure of effectiveness of the compliant motion control is the *mechanical admittance* Y defined as [18]

$$Y = \frac{v_f}{F} \quad (10)$$

where v_f is the end-effector velocity and F is the contact force, both at the point of interaction. A large admittance corresponds to a rapid motion induced by applied forces; while a small admittance represents a slow reaction to contact forces. Based on the above discussions, the force compensator transfer-function $K(s) = \frac{v_f(s)}{e(s)}$ is expressed as the product

$$K(s) = \frac{1}{s} \cdot Y(s) \quad (11)$$

where the admittance $Y(s)$ relates the force error e to the end-effector velocity perturbation $v_f(s)$; i.e., $Y(s) = \frac{v_f(s)}{e(s)}$. For a known environmental stiffness, an admittance $Y(s)$ can be constructed to achieve a desirable force response with small or zero error, low overshoot, and rapid rise time. However, the same admittance typically exhibits sluggish response in contact with softer environments, and goes unstable when contacting stiffer environments. In other words, because different environments have diverse stiffness which can vary over several orders of magnitude, a fixed admittance design based on a nominal environment leads to non-uniform dynamic performance and often instability. To overcome this problem, we propose *adaptive admittance control* where the parameters of the admittance $Y(s)$ are tuned automatically on-line based on the force tracking performance of the system. This approach provides stable and uniform performance under gross variations in the environmental stiffness.

In this section, we consider two classes of adaptive admittances that can be used for force or proximity control within the compliant motion control framework. The second-order admittance leads to an adaptive PID force compensator, while the first-order admittance leads to an adaptive PI force compensator.

4.1 Adaptive PID Force Compensator

In this section, an adaptive second-order admittance control scheme will be developed to accomplish force control within the compliant motion framework.

Consider the admittance-based compliant control system shown in Figure 4. Let us choose a second-order admittance model as

$$Y(s) = k_d s^2 + k_p s + k_i \quad (12)$$

resulting in the following force compensator

$$K(s) = \frac{1}{s} \cdot Y(s) = k_d s + k_p + \frac{k_i}{s} \quad (13)$$

where $\{k_p, k_i, k_d\}$ are the proportional, integral, and derivative force feedback gains, respectively. This leads to the force feedback law

$$x_f = k_d \frac{d}{dt} e + k_p e + k_i \int_0^t e dt \quad (14)$$

which implies that the position perturbation x_f due to cent act force is in direct proportion to the rate-of-change of force error $\frac{d}{dt} e$, the instantaneous value of force error e , and the time-integral of force error $\int_0^t e dt$. Therefore, the force control law contains information about the past history [through $\int_0^t e dt$], the present value [through e], and the future trend [through $\frac{d}{dt} e$] of the force tracking performance of the system.

For the purpose of control law development, we consider the control signal x_f to be comprised of proportional and derivative terms in $\{e, \dot{e}\}$ together with an auxiliary signal $g(t)$ which contains the integral term, that is

$$x_f(t) = g(t) + k_p(t)e(t) + k_d(t)\dot{e}(t) \quad (15)$$

where $\{k_p(t), k_d(t)\}$ are the adaptive proportional and derivative force feedback gains, respectively. On applying the control law (15) to the system shown in Figure 4, and noting that F_r, k_e , and x_e are constant, we obtain the force error dynamics as

$$\ddot{e} + [a + bk_e k_d]\dot{e} + [b' + bk_e k_p]e = b'[F_r - F_x] - bk_e g \quad (16)$$

where F_x is defined in (5). Equation (16) represents the "adjustable system" in the model-reference adaptive control (MRAC) framework. Suppose that the *desired* behavior of the force tracking-error e_m is specified as

$$\ddot{e}_m + 2\zeta\omega\dot{e}_m + \omega^2 e_m = 0 \quad (17)$$

where ζ and ω are the user-specified damping ratio and undamped natural frequency of the force error dynamics. Equation (17) constitutes the "reference model" within the MRAC framework. Following Appendix 1, the adaptation laws for $\{g(t), k_p(t), k_d(t)\}$ which ensure

that the solution $e(t)$ of the error dynamics (16) tends asymptotically to the solution $e_m(t)$ of the reference model(17) are given by

$$\begin{aligned} q(t) &= w_p e(t) + w_d \dot{e}(t) \\ g(t) &= g(0) + \alpha_1 \int_0^t q(t) dt + \alpha_2 q(t) \\ k_p(t) &= k_p(0) + \beta_1 \int_0^t q(t) e(t) dt + \beta_2 q(t) e(t) \\ k_d(t) &= k_d(0) + \gamma_1 \int_0^t q(t) \dot{e}(t) dt + \gamma_2 q(t) \dot{e}(t) \end{aligned} \quad (18)$$

where (w_p, w_d) are the positive position and velocity weighting factors, $(\alpha_1, \beta_1, \gamma_1)$ are the positive integral adaptation gains, $(\alpha_2, \beta_2, \gamma_2)$ are the positive or zero proportional adaptation gains, and $[g(0), k_p(0), k_d(0)]$ are the positive initial values chosen to provide appropriate initial position perturbation signal and initial proportional and derivative gains for the control system. The force control scheme is shown in Figure 5. Using (18), the force control law (15) can be written as

$$x_f(t) = x_f(0) + k_p^*(t) e(t) + k_i^* \int_0^t e(t) dt + k_d^*(t) \dot{e}(t) \quad (19)$$

where $k_p^*(t) = \alpha_1 w_d + \alpha_2 w_p + k_p(t)$ is the adaptive proportional gain, $k_i^* = \alpha_1 w_p$ is the constant integral gain, $k_d^*(t) = \alpha_2 w_d + k_d(t)$ is the adaptive derivative gain, and $x_f(0) = g(0)$. It is seen that the position perturbation $x_f(t)$ due to contact force is generated by a 1'11) controller driven by the force tracking-error $e(t)$, where the controller is composed of a constant-gain 1'111) term and an adaptive-gain PID term.

From a practical point of view, the contact force F' measured by the force/torque sensor is often a noisy signal and hence direct differentiation of this signal to obtain \dot{e} is undesirable. Two alternative solutions are available to overcome this problem. The first solution is to filter the measured force signal F' in order to remove the high-frequency noise superimposed on F' . Oftentimes, a simple first-order low-pass filter is sufficient to remove the noise. The "filtered" force signal \hat{F}' can then be differentiated and used in the force control law (15). The second solution is to replace \dot{e} by $-k_e \dot{x}$, as suggested by $F' = k_e(x - x_e)$, where F'_r is constant. Also note that since k_e is an unknown positive constant, it can be absorbed in the adaptation gains and in the weighting factors. Furthermore, in the analysis so far, we have neglected the dynamical effects of the environment. To ensure robustness in the presence of this unmodeled dynamics, we slightly modify the adaptation laws (18) using the a-modification terms [43]. Thus, the modified adaptation laws using the velocity signal \dot{x} are given by

$$\begin{aligned} x_f(t) &= g(t) + k_p(t) e(t) + k_v(t) \dot{x}(t) \\ g(t) &= g(0) + \alpha_1 \int_0^t q(t) dt + \alpha_2 q(t) + \sigma_1 \int_0^t g(t) dt \end{aligned}$$

$$\begin{aligned}
k_p(t) &= k_p(0) + \beta_1 \int_0^t q(t)e(t)dt + \beta_2 q(t)e(t) + \sigma_2 \int_0^t k_p(t)dt \\
k_v(t) &= k_v(0) + \lambda_1 \int_0^t q(t)dt + \lambda_2 q(t)\dot{x}(t) + \sigma_3 \int_0^t k_v(t)dt \\
q(t) &= w_p e(t) + w_v \dot{x}(t)
\end{aligned} \tag{20}$$

where $\lambda_1 = \gamma_1 k_e$, $\lambda_2 = \gamma_2 k_e$, $w_v = w_d k_e$ and $\sigma_1, \sigma_2, \sigma_3$ are small positive constants. The addition of the σ -modification terms enhances robustness in the presence of the unmodeled dynamics, at the price of a residual force tracking-error of order (σ) .

We conclude that the adaptive second-order admittance control scheme developed in this section for generating the position perturbation is extremely simple and computationally very efficient. As a result, the control scheme can be implemented for real-time force control with a high sampling rate, which is critical for closed-loop stability of force control loops that contain typically large environmental stiffness k_e . Furthermore, since the controller terms do not require knowledge of x_e and k_e and are adjusted on-line based on the force tracking performance through \dot{e} , the controller can rapidly adapt itself to gross changes in the environmental parameters x_e and k_e .

4.2 Adaptive PI Force Compensator

In this section, an adaptive first-order admittance control scheme will be developed for force control within the compliant motion framework.

Consider the admittance-based compliant control system shown in Figure 4, with the first-order admittance model

$$Y(s) = k_p s + k_i \tag{21}$$

resulting in the PI force compensator

$$K(s) = \frac{1}{s} \cdot \{ \} (s) = k_p - 1 ; - \tag{22}$$

and the force feedback law

$$x_f = k_p e + k_i \int_0^t e dt \tag{23}$$

where $\{ k_p, k_i \}$ are the proportional and integral force feedback gains, respectively. In comparison with the second-order admittance model (12) used in Section 4.1, the first-order admittance model (21) has the advantage of *not* requiring the rate-of-change of the force error \dot{e} , which is a noisy signal. As a result, the PI control scheme is much simpler to implement in practice. However, the price paid for this simplicity is that there are now insufficient adjustable gains in the compensator to ensure that the error dynamics (16) follows an arbitrary user-specified reference model (17). In this case, the force feedback gains are chosen to ensure merely that the error dynamics is asymptotically stable, so that $e(t) \rightarrow 0$ as $t \rightarrow \infty$.

Applying the PI control law (23) to the system shown in Figure 4, we obtain the dynamic model of the force tracking-error as

$$\ddot{e} - (a - 1) \dot{e} - (b' - 1) b k_e k_p e - b k_e k_i \int_0^t e dt = b' [I_r' - I_x'] \quad (24)$$

where $I_x' = k_e \left[\frac{b}{v} x_r - x_e \right]$ is the constant contact force solely due to x_r . It is seen that the coefficient of \dot{e} in the error dynamics (24) is constant and cannot be affected by the controller gains $\{k_p, k_i\}$. This is expected since the force compensator does not have any active damping term $k_d \dot{e}$ to contribute to the passive damping “ a ” of the system. Now, we need to find the adaptation laws for the proportional gain $k_p(t)$ and the integral gain $k_i(t)$ to ensure that (24) represents an asymptotically stable system.

To simplify the stability analysis, we choose the integral gain k_i as a constant and employ an adaptation law for the proportional gain k_p as a nonlinear function of the force tracking-error e . We adopt the Lyapunov approach to investigate the stability of the third-order nonlinear error differential equation (24). For a class of third-order nonlinear differential equations such as (24), Barbashin [44] has obtained specific stability criteria using a Lyapunov analysis; [see Appendix II]. Applying Barbashin’s method to the error dynamics (24) yields the following three stability conditions:

$$\begin{aligned} \text{(i)} \quad & a > 0 \\ \text{(ii)} \quad & b k_e k_i \left[\int_0^t e dt \right]^2 > 0 \quad \rightarrow \quad k_i > 0 \\ \text{(iii)} \quad & a [b' - 1] b k_e k_p - b k_e k_i > 0 \quad \rightarrow \quad k_i < a \left[k_p + \frac{b'}{b k_e} \right] \end{aligned}$$

Thus, we conclude that the stability of the nonlinear differential equation (24) is guaranteed provided that

$$0 < k_i < a \left[k_p + \frac{b'}{b k_e} \right] \quad (25)$$

Note that conservative estimates of the attenuation factor a and the forward path gain $\frac{b k_e}{v}$ can readily be obtained from the open-loop response of the contact force I' to the step reference position x_r with no force feedback ($x_f = 0$). Furthermore, observe that closed-loop stability is attained for *all* environmental stiffness k_e provided that the following relationship holds between the proportional and integral gains

$$0 < k_i < a k_p \quad (26)$$

It is seen that the stability condition (26) does not contain the stiffness of the environment k_e . One viable choice for the proportional gain k_p as a function of the force tracking-error e is given by

$$k_p(t) = k_{p0} + a e^2(t) \quad (27)$$

where k_{p0} is the positive constant value chosen for k_p when $e = 0$, and α is the positive constant adaptation gain chosen by the user to reflect the sensitivity of k_p to e . Notice that the adaptive term αe^2 contributes only to the transient response by increasing the proportional gain k_p so as to reduce the tracking-error e . When e is small, the effect of αe^2 is diminished and k_p restores to its initial value k_{p0} . On substituting for k_p in Barbashin's stability condition (25), we obtain

$$0 < k_i < a \left[k_{p0} + \alpha e^2 + \frac{b'}{bk_c} \right] \quad (28)$$

Therefore, provided that the controller gains are chosen such that

$$0 < k_i < a \left[k_{p0} + \frac{b'}{bk_{e1}} \right] \quad (29)$$

the stability of the closed-loop compliant control system is guaranteed. Figure 6 shows a block diagram of the adaptive PI force control scheme.

Equation (27) implies that

$$\dot{k}_p(t) = 2\alpha e(t)\dot{e}(t) \quad (30)$$

This means that the rate-of-change of the proportional gain k_p is in direct proportion to the size of the tracking-error e and the rate-of-change of e . To illustrate qualitatively the adaptation of the controller gain k_p , consider a typical force response and the corresponding phase plot shown in Figures 7a and 7b. The force response and phase plot consist of four segments AB, BC, CD, and DE; the segments are repeated periodically after E with decreasing amplitude. In segments BC and DE, c and \dot{e} have the same sign [in BC, $c < 0$, $\dot{e} < 0$; in DE, $c > 0$, $\dot{e} > 0$], and these segments represent *unfavorable trends* since the force error is negative for BC (positive for DE) and is decreasing further (increasing further). In these cases, $e\dot{e} > 0$ and from (30), $\dot{k}_p > 0$, and the controller gain k_p increases. In segments AB and CD, c and \dot{e} have opposite signs [in AB, $c > 0$, $\dot{e} < 0$; in CD, $c < 0$, $\dot{e} > 0$] and these segments represent *favorable trends* since the force error is positive in AB (negative in CD) and is decreasing (increasing) toward zero. In these cases, $e\dot{e} < 0$ and $\dot{k}_p < 0$ which means that k_p will decrease. We conclude that when the force response has an unfavorable trend, the proportional gain increases rapidly to correct the response; whereas during a favorable trend, the gain decreases since no corrective action is called for. Notice that the proportional gain will adjust continuously until the steady-state is reached when $c = \dot{e} = 0$ and k_p assumes the specified constant value k_{p0} .

Finally, it is interesting to rederive the Lyapunov stability condition (26) in the special case of constant k_p, k_i using the classical root locus analysis. With constant k_p and k_i and $K(s) = k_p + \frac{k_i}{s}$, $\frac{k_p s + k_i}{s}$, the variations of closed-loop poles as the environmental stiffness k_e varies from 0 to ∞ are shown in Figure 8 for the case where the position-controlled robot is overdamped. It is seen that as k_e increases, one closed-loop pole moves toward

the compensator zero at $-k_i/k_p$ while the remaining two closed-loop poles move toward the asymptotes at $s = \sigma$; where from the root locus method $\sigma = \frac{-a + k_i/k_p}{2}$. Therefore, provided that $k_i < ak_p$, we obtain $\sigma < 0$ and the root loci stay entirely in the left-half plane and closed-loop stability is guaranteed for all k_e . Notice that the condition $k_i < ak_p$ was obtained earlier in (26) using a Lyapunov analysis.

in conclusion, using the first-order admittance control scheme

$$x_f(t) = [k_{p0} + \alpha e^2(t)]e(t) + k_i \int_0^t e(t)dt \quad (31)$$

we ensure that the closed-loop force control system is always stable when the robot is in contact with an environment having an unknown stiffness coefficient k_e . It is interesting to note that the mechanical realization of the force control law (31) is a nonlinear spring in series with a linear damper as shown in Figure 9. In this case, we have the force-displacement relationships

$$\begin{aligned} e &= k(x_f - x) = b\dot{x} \\ x_f &= \frac{1}{k}e + \frac{1}{b} \int_0^t e dt \end{aligned} \quad (32)$$

with $k = \frac{1}{k_p}$ and $b = \frac{1}{k_i}$.

Finally, we discuss "the steady-state setpoint regulation and disturbance rejection characteristics of the force control schemes developed in this section. Consider the admittance-like PID and 1st force control systems shown in Figures 5 and 6. Since the closed-loop system is asymptotically stable, when the step force setpoint F_r^* and the constant force disturbance F_d are applied to the system, the integral of force error $\int_0^t e(t)dt$ which is a system state-variable reaches a constant value in the steady-state. Hence $\frac{d}{dt} \left[\int_0^t e(t)dt \right] = e(t)$ tends to zero as $t \rightarrow \infty$; that is, the contact force F tracks the force setpoint F_r^* and rejects the force disturbance F_d when the steady-state is reached. Furthermore, when the system parameters $\{a, b, b', k_e\}$ or the compensator gains $\{k_p, k_i, k_d\}$ undergo gross and arbitrary variations, the control system is *robust* in the sense that the setpoint regulation and disturbance rejection characteristics are retained, *provided that the closed-loop system remains stable*. Note that while these steady-state properties are preserved, the closed-loop system may exhibit unacceptable transient responses for certain values of system parameters or compensator gains. We note that the robust setpoint regulation and disturbance rejection characteristics are due to the presence of the integral term in the force compensator. These inherent features of integral control make it a vital component in any practical explicit force control scheme.

5 Adaptive Compliance Control

In this section, we consider the implicit force control system shown in Figure 2 in which the reference position x_r is used as a command to control the contact force F during constrained

tasks. This is accomplished by establishing a desirable position-force ($x_r - F'$) relationship through an appropriate choice of the compensator $K(s)$. Compliance control accepts the position command x_r as input and produces the contact force F' as output, and does not use any force setpoint. This is in contrast to admittance control discussed in Section 4, in which the force setpoint F'_r is commanded to control the contact force F' , and the force error e is mapped to the position perturbation x_f .

In subsequent sections, the conventional compliance compensator is first reviewed briefly from the stability point of view. A compensator modification is then proposed to enhance closed-loop stability, and simple methods for compensator adaptation are developed to improve system performance.

5.1 Structure of Compliance compensator

The most common implementation of the compliance compensator $K(s)$ is the first-order lag filter [7, 10, 19, 20]

$$K(s) = \frac{x_f(s)}{F'(s)} = \frac{1}{k_d s + k_s} \quad (33)$$

where k_d and k_s are positive constants. In this case, the trajectory perturbation x_f due to the contact force F' obeys the differential equation

$$k_d \dot{x}_f(t) + k_s x_f(t) = F'(t) \quad (34)$$

Therefore, the compensator "behaves" like a spring with stiffness coefficient k_s in series with a damper having friction coefficient k_d . Note that if a pure gain is used instead of the lag compensator (i.e., $k_d = 0$) a spring with no damper is realized, which yields an undesirable response since the manipulator clamping B_m can not be altered by the compensator. If an integrator is used instead of the lag compensator (i.e., $k_s = 0$), the position-accommodation or damping control scheme [1] is retrieved which has an undesirable feature due to lack of a spring action to restore the reference position when $F' = 0$. Therefore, the lag filter combines the attractive features of both the spring and the damper in a single compensator.

The performance and stability of the compliant control system with $K(s) = \frac{1}{k_d s + k_s}$ has been studied in detail by Lawrence and Stoughton [10]. They derive a set of stability boundaries in the (k_s, k_d) plane that divide the plane into a stable region and an unstable region of operation. The instability phenomenon becomes evident by considering the root locus behavior of the closed-loop system. For a given compensator $K(s) = \frac{1}{k_d s + k_s}$, the loci of closed-loop poles as a function of the environmental stiffness k_e are shown in Figure 10, where it is assumed that the manipulator poles are slightly overdamped. It is seen that as the value of k_e is increased from zero, one pole moves on the negative real-axis, while the remaining two poles move on the real-axis toward a breakaway point, the poles then coalesce and subsequently become complex conjugates, and finally for $k_e > k_{e,max}$ the poles move toward the unstable region (right-half plane) on two asymptotes which intersect the real axis at an

angle of 3.60° . We conclude that the compliant control system using the lag compensator will become unstable when contacting environments with high stiffness $k_e > k_{e,max}$. The value of $k_{e,max}$ depends on the compensator parameters (k_s, k_d) , as well as on the numerical values of the manipulator parameters (a, b, U) . Notice that if the second-order impedance filter $K(s) = \frac{1}{ms^2 + ds + k}$ is used instead of the first-order compensator (33), the closed-loop system will be less stable due to the additional 90° phase lag introduced by $K(s)$. This is also evident by noting that the angle of root locus asymptotes will change from $\pm 60^\circ$ to $\pm 145^\circ$, thus forcing the closed-loop poles to move sooner into the right-half plane.

In order to maintain system stability under high environmental stiffness, we propose a simple modification to the basic compliance control scheme of equation (33). Consider the conventional compliance compensator $1/(k_d s + k_s)$, and add in parallel the force feedforward gain k_f as shown in Figure 11 to yield the *lag-plus-feedforward compensator*

$$K(s) = k_f + \frac{k}{k_d s + k_s} = \frac{\alpha s + 1}{k_d s + k_s} \quad (35)$$

where k is the gain of the lag term, $\alpha = k_f k_d$ and $\beta = k_f k_s + k$. It is seen that the introduction of the feedforward gain k_f has given rise to a compensator zero at $s = -\beta/\alpha$. The proposed compliance compensator (35) has the simple mechanical realization of the spring-damper-spring system shown in Figure 12. For this mechanical system, we have the force-displacement relationship

$$F = \frac{1}{k_f} (x_f - x) = \frac{k_s}{k} x + \frac{k_d}{k} \dot{x} \quad (36)$$

which yields the input-output model

$$\frac{x_f}{F} = k_f + \frac{k}{k_d s + k_s}$$

Let us now investigate the stability of the closed-loop system using the proposed compliance compensator (35). Figure 13 shows the root loci of the closed-loop system with the environment stiffness k_e as a parameter. It is seen that as k_e increases, one closed-loop pole moves toward the compensator zero at $s = -\beta/\alpha$, while the remaining two poles move on the real axis, coalesce, and then break away and move toward two asymptotes which are perpendicular to the real-axis at $s = \sigma$. Therefore, the effect of the additional compensator zero (produced by the feedforward gain k_f) is to 'pull' the root loci to the stable left-half plane by changing the angle of asymptotes from 60° to 90° , thus enhancing the stability of the compliant control system. It is seen that provided $\sigma < 0$, the closed-loop poles are stable for all values of k_e , and thus the compliant control system is stable *regardless of the environmental stiffness*. The value of σ is obtained as

$$\sigma = \frac{-a - k_s/k_d - 1 - \beta/\alpha}{2}$$

hence for large-stiffness stability, we require $\sigma < 0$; that is

$$\frac{\beta}{\alpha} < a + \frac{k_s}{k_d} \quad (37)$$

This result can be verified by applying Routh's criterion to the closed-loop characteristic polynomial $A(s)$ obtained from

$$1 + \frac{b}{s^2 + as + b} \cdot k_c \cdot \frac{cs - 1}{k_d s + k_s} = 0$$

as

$$\Delta(s) = k_d s^3 - 1 [k_s - 1 a k_d] s^2 - 1 [a k_s + b' k_d - 1 \alpha b k_c] s - 1 [b' k_s - 1 \beta b k_c] \quad (38)$$

When the parameters $(a, b, b', k_d, k_s, \alpha, \beta)$ are positive, for stability we only require

$$[k_s - 1 a k_d][a k_s + b' k_d + \alpha b k_c] > k_d [b' k_s - 1 \beta b k_c] \quad (39)$$

which leads to

$$\beta < \beta_{max} = \frac{a k_s^2}{b k_c k_d} + \frac{a^2 k_d k_s}{b k_c k_d} - 1 + \frac{a b' k_d^2}{a - 1} \frac{k_s}{k_d} \quad (40)$$

It is seen that for soft environments, β_{max} is high; whereas for hard environments, $\beta_{max} \rightarrow \alpha \left[a + \frac{k_s}{k_d} \right]$. Therefore, to ensure stability, it is sufficient to have

$$\beta < \alpha \left[a + \frac{k_s}{k_d} \right] \quad (41)$$

which was obtained in (37) using the root locus method. A more conservative sufficient condition for closed-loop stability is found to be

$$\frac{\beta}{\alpha} < \frac{k_s}{k_d} \quad (42)$$

Note that $\frac{\beta}{\alpha} < \frac{k_s}{k_d}$ is a *sufficient* but not a necessary condition for stability, and it is therefore more stringent than need be. Since the compensator zero at $s = -\beta/\alpha$ is closer to the origin than the compensator pole at $s = -k_s/k_d$ when inequality (42) is satisfied, $K(s)$ is a *phase-lead* compensator. It is by virtue of the phase-lead that closed-loop stability is enhanced by the proposed compensator $\frac{\alpha s + \beta}{k_d s + k_s}$ compared to the conventional lag compensator $\frac{k_s}{k_d s + k_s}$. Note that the compensator zero also speeds up the response of the compliant control system, since the force feedforward term $k_f J'$ produces a corrective action spontaneously while the lag output is building up. It is important to note that the compensator coefficients $(k_s, k_d, \alpha, \beta)$ affect all four coefficients of the closed-loop characteristic polynomial $A(s)$, and therefore the compensator $K(s)$ can be chosen such that $A(s)$ has some desirable stable roots.

1A us now examine the relationship between the reference position trajectory x_r and the resulting contact force F . Without loss of generality and to simplify the analysis, the world frame is defined to be on the environment so that $x_e = 0$. From Figure 11, we have

$$\frac{F(s)}{x_r(s)} = \frac{\frac{bk_e}{s^2 + as + b'}}{\frac{bk_e}{s^2 + as + b'} \cdot \frac{\alpha s + \beta}{k_d s + k_s}} \cdot \frac{bk_e(k_d s - 1)k_s}{(s^2 + as + b')(k_d s + k_s) + bk_e(\alpha s + \beta)} \quad (43)$$

Equation (43) represents a third-order system with poles in the stable left-half plane and a zero at $s = -k_s/k_d$. For a step position command $x_r(t) = x_{ss}$, the steady-state contact force is given by

$$F_{ss} = \lim_{s \rightarrow 0} F(s) = \frac{bk_e k_s}{b'k_s + bk_e \beta} x_{ss} = \frac{1}{\frac{\beta}{k_s} + \frac{b'}{bk_e}} x_{ss} \quad (44)$$

Therefore, the contact force F can be controlled directly by the position command x_r for a given k_e and $K(s)$. Equation (44) implies that in the steady-state, the compliant control system behaves like a pure spring with stiffness coefficient $k_{ap} = \left[\frac{\beta}{k_s} + \frac{b'}{bk_e} \right]^{-1}$, which is the equivalent stiffness of two springs with stiffness coefficients $\frac{k_s}{\beta}$ and $\frac{bk_e}{b'}$ connected in series. Note that $\frac{k_s}{\beta}$ is the equivalent stiffness of the series combination of the two springs $\frac{1}{k_f}$ and $\frac{k_s}{k}$ present in the compliance compensator $K(s)$, since $\frac{1}{\frac{1}{k_f} + \frac{1}{k_s}} = \frac{k_s}{k_f k_s + k} = \frac{k_s}{\beta}$. As a result, in the steady-state, the compliant control system behaves like three springs connected in series: $\frac{bk_e}{b'}$ representing the robot-environment stiffness in series with k_f^{-1} and $k_s k^{-1}$ representing the compensator, so that $F_{ss} = [b'(bk_e)^{-1} - 1/k, -1/k k_s^{-1}]^{-1} x_{ss}$. Note that the compliance compensator $\frac{\alpha s + \beta}{k_d s + k_s}$ acts like a spring $\frac{k_s}{\beta}$ to *change* the robot-environment stiffness $\frac{bk_e}{b'}$ appropriately and thus provide the desirable apparent stiffness k_{ap} .

From equation (44), the steady-state contact force F_{ss} can be expressed as

$$F_{ss} = \frac{k_s}{\beta + \frac{b'}{bk_e} k_s} x_{ss} \quad (45)$$

It is seen that given the environmental stiffness k_e and the robot parameters (b, U), the compensator parameters (β, k_s) can be chosen such that the $x_r - F$ relationship (45) matches the user-specified target model

$$F_m = k_m x_{ss} \quad (46)$$

where F_m and k_m are the desired contact force due to x_{ss} and the desired apparent stiffness, respectively. On comparing equations (45) and (46) and setting $k_s = 1$, we obtain

$$\beta = \frac{1}{k_m} - \frac{b'}{bk_e} \quad (47)$$

The compliance compensator $K(s)$ with β given by (47) ensures that the robot-environment interaction emulates the target model (46) in the steady-state. Note that for stiff environments, equation (45) reduces to

$$F_{ss} \approx \frac{k_s}{\beta} x_{ss} \quad (48)$$

and hence the apparent stiffness becomes $k_{ap} = k_s/\beta$ which is independent of k_e . It is seen that the contact force F_{ss} is directly proportional to k_s and inversely proportional to β . Hence we can set $k_s = 1$ and $\beta = \frac{1}{k_e}$ to emulate the target model (46).

Finally, we make the following observations regarding the proposed compliance compensator:

1. When $k_s = 0$ in the compliance compensator $K(s) = \frac{\alpha s + \beta}{k_d s + k_s}$, the PD force compensator $\left[\frac{\alpha}{k_d}\right] + \left[\frac{\beta}{k_d}\right] \cdot \frac{1}{s}$ is retrieved, which is discussed in Section 4.2. From (44), it is seen that in this case $F_{ss} = 0$; i.e., the PD compensator achieves zero steady-state contact force, as expected.
2. The compensator $K(s) = \frac{\alpha s + \beta}{k_d s + k_s}$ can be viewed as the low-pass filter $\frac{1}{k_d s + k_s}$ in cascade with the proportional-derivative (PD) controller $\alpha s + \beta$. Hence, in effect, the measured contact force F passes through the low-pass filter to produce the "filtered force" $\hat{F} = \frac{F}{k_d s + k_s}$, which is then operated on by the PD controller to generate the position perturbation $x_f = \alpha \frac{d}{dt} \hat{F} + \beta \hat{F}$. Alternatively, the compliance compensator can be expressed as $K(s) = k_p^* + \frac{1}{1 + T^* s} k_r^* s$, where $k_p^* = \frac{\beta}{k_s}$, $k_r^* = \frac{\alpha - \beta k_d/k_s}{k_s}$, and $T^* = \frac{k_d}{k_s}$. This represents a "proportional-plus-filtered-derivative" controller, in which the low-pass filter $\frac{1}{1 + T^* s}$ removes the high-frequency noise superimposed on the measured contact force before differentiation. Note that the built-in low-pass filter is an attractive feature of this compliance compensator.
3. The dynamical model of the compliance compensator relating the input F to the output x_f is given by

$$k_d \frac{d}{dt} x_f(t) + k_s x_f(t) = \alpha \frac{d}{dt} F(t) + \beta F(t) \quad (49)$$

It is seen that the position perturbation $x_f = x_r - x_e$ is related to the contact force F by a first-order differential equation, which also contains $\frac{dF}{dt}$. The force derivative term $\frac{dF}{dt}$ due to the feedforward gain k_f results in a predictive corrective action and makes the system more responsive, especially when F is small but is changing rapidly, e.g., at impact and initial phase of contact. This utilization of information on the future trend of contact force enhances system stability and improves dynamic performance [see, e.g., 21]. Notice that when the end-effector is in contact with a hard environment,

the relationship between the position command x_r and the contact force F is found from equation (43) as

$$\frac{F'(s)}{x_r(s)} = [K(s)]^{-1} = \frac{k_d s + k_s}{\alpha s + \beta}$$

or

$$k_d \dot{x}_r(t) + k_s x_r(t) = \alpha \dot{F}(t) + \beta F(t)$$

which is a first-order differential equation containing both $\dot{x}_r(t)$ and $F(t)$.

5.2 Stability-Based Adaptive Compliance Compensator

Consider the compliant motion control system shown in Figure 1. The differential equation relating the contact force F to the reference position x_r is found to be

$$k_d \frac{d^3 F'}{dt^3} + [k_s + a k_d] \frac{d^2 F'}{dt^2} + [a k_s + b' k_d + \alpha b k_e] \frac{d F'}{dt} + [b' k_s + \beta b k_e] F' = [b k_e k_d] \frac{d x_r}{dt} + [b k_e k_s] x_r \quad (50)$$

Now, to apply a constant force on the environment, the reference position x_r will be chosen to penetrate into the environment by a constant amount. Hence, we can set $\frac{d x_r}{dt} = 0$ and investigate the stability of the third-order differential equation (50) using a Lyapunov approach. In order to improve the performance of the compliant control system, it is suggested that the compensator gain β be a nonlinear function of the contact force F . On applying Barbashin's theorem to the third-order nonlinear differential equation (50) with $\frac{d x_r}{dt} = 0$ [see Appendix 11], the following three stability conditions are obtained:

- (i) $\frac{k_s + a k_d}{k_d} > 0$
- (ii) $\frac{b' k_s + b k_e \beta}{k_d} F'^2 > 0$
- (iii) $\left[\frac{k_s + a k_d}{k_d} \right] \left[\frac{a k_s + b' k_d + \alpha k_e b}{k_d} \right] - \frac{d}{d F'} \left[\frac{b' k_s + b k_e \beta}{k_d} F' \right] > 0$

where it is assumed that the parameters (k_d, k_s, α) of the compensator are fixed and the parameter β is a function of the contact force F . Conditions (i) and (ii) are satisfied when the compensator parameters $(k_d, k_s, \alpha, \beta)$ are chosen to be positive. Condition (iii) simplifies to

$$\left[\beta + F' \frac{d\beta}{dF'} \right] < \frac{1}{b k_e} \left[a \frac{k_s^2}{k_d} + a b' k_d + a^2 k_s \right] + \left[\alpha a + \alpha \frac{k_s}{k_d} \right] \quad (51)$$

It is seen that when β is a constant, Barbashin's stability condition (51) reduces to Routh's stability condition (40) obtained in Section 5.1.

Suppose that we wish to emulate the user-specified steady-state *static* target interaction model

$$F'_m = k_m x_{ss} \quad (52)$$

Then, we can choose the compensator gain β as a function of deviation of the actual contact force F' from its desired value F'_m . Now, β must be chosen such that $\beta^{-1} F' \frac{d\beta}{dF'}$ has a finite upper-bound which satisfies the stability inequality (51). A viable choice of β is

$$\beta = \beta_0^{-1} \gamma [1 + \exp((F'_m - F')/\tau)] \quad (53)$$

where γ and τ are positive constants specified by the user, and β_0 is the nominal value of β that produces the target model stiffness k_m . With this choice of β , when $F' > F'_m$ the value of β increases, and this in turn decreases the apparent stiffness k_{ap} and reduces the contact force F' . Similarly, when $F' < F'_m$, β decreases to increase the apparent stiffness and thus increases the contact force. Note that since $\frac{d\beta}{dF'} \propto \exp[(F'_m - F')/\tau]$, γ reflects the "rate-of-adaptation" or sensitivity of β to F' . In Appendix 111, it is shown that with this choice of β , the expression $\beta^{-1} F' \frac{d\beta}{dF'}$ is upper-bounded by β_m , that is

$$\beta^{-1} F' \frac{d\beta}{dF'} < \beta_m \quad (54)$$

where $\beta_m = \beta_0^{-1} \gamma [1 + \exp(F'_m/\tau - 2)]$. Hence, from inequalities (51) and (54), we conclude that a sufficient condition for closed-loop stability is given by

$$\beta_m < \alpha a + \alpha \frac{k_s}{k_d} \quad (55)$$

A more conservative sufficient, but not a necessary, condition for stability is found to be

$$\frac{\beta_m}{\alpha} < \frac{k_s}{k_d} \quad (56)$$

Inequalities (55) and (56) are similar to the conditions (41) and (42) obtained in Section 5.1 for a constant gain compensator. Inequality (56) imposes a simple condition which guarantees closed-loop stability without any knowledge of the robot parameters (a, b, b') or the environmental stiffness k_e .

In order to appreciate the operation of the compensator gain β , from (53) we obtain

$$\frac{d\beta}{dt} = \left\{ \frac{\gamma}{\tau} \exp[(F'_m - F')/\tau] \right\} \cdot \frac{dF'}{dt} \quad (57)$$

From (57), it is seen that $\frac{d\beta}{dt}$ and $\frac{dF'}{dt}$ have the same sign. This implies that when F' is increasing ($\frac{dF'}{dt} > 0$), β also increases in order to reduce F' to F'_m . Similarly, when F' is decreasing ($\frac{dF'}{dt} < 0$), β also decreases so as to increase F' to F'_m . We conclude that the adaptation law given by (53) is expected to improve the performance of the compliant control system.

5.3 MIA-based Adaptive Compliance Compensator

Consider the compliant motion control system shown in Figure 11. In this section, we develop a simple MIA-based adaptive compliance control scheme to ensure that the *dynamic* model relating the reference position x_r to the contact force F emulates a user-specified target dynamic model. This enables the robot to exhibit the *same* response characteristics, e.g., apparent stiffness and time-constant, when contacting environments with different stiffnesses.

From equation (50), the *actual interaction dynamics* representing the manipulator-environment interaction can be described by the third-order differential equation

$$\frac{k_d}{bk_e} \frac{d^3 F}{dt^3} + \left[\frac{k_s + ak_d}{bk_e} \right] \frac{d^2 F}{dt^2} + \left[\frac{ak_s + b'k_d}{bk_e} + \alpha \right] \frac{dF}{dt} + \left[\frac{b'k_s}{bk_e} + \beta \right] F = k_d \frac{dx_r}{dt} + k_s x_r \quad (58)$$

The numerical value of k_d is often chosen to be small to filter out the high-frequency noise superimposed on the contact force. Furthermore, $\frac{1}{k_e}$ is often a small number in practice. Therefore, for adaptive control development [43], the third-order full dynamic model (58) can be approximated by the first-order reduced dynamic model

$$\left[\frac{ak_s + b'k_d}{bk_e} + \alpha \right] \dot{F}(t) + k_s x_r(t) \quad (59)$$

or

$$\frac{\dot{F}(s)}{x_r(s)} = \frac{k_d s + k_s}{\left[\frac{ak_s + b'k_d}{bk_e} + \alpha \right] s + \left[\frac{b'k_s}{bk_e} + \beta \right]} \quad (60)$$

Notice that the reduced-order model (59)-(60) can alternatively be obtained by ignoring the dynamics of the position-controlled robot. Equations (59) and (60) can be written in terms of the "filtered" contact force $\hat{F} = \frac{1}{k_d s + k_s} F$ as

$$\left[\frac{ak_s + b'k_d}{bk_e} + \alpha \right] \frac{d}{dt} \hat{F}(t) + \left[\frac{b'k_s}{bk_e} + \beta \right] \hat{F}(t) = x_r(t) ; \quad \frac{\hat{F}(s)}{x_r(s)} = \frac{1}{\left[\frac{ak_s + b'k_d}{bk_e} + \alpha \right] s + \left[\frac{b'k_s}{bk_e} + \beta \right]} \quad (61)$$

On applying a reference position command x_r with constant final value, the contact force F responds with the time-constant $\tau = \frac{ak_s + b'k_d + bk_e \alpha}{b'k_s + bk_e \beta}$ and presents the steady-state apparent stiffness $k_{ap} = \frac{b'k_s}{b'k_s + bk_e \beta}$. It is seen that both the response time and the apparent stiffness are functions of the environmental stiffness k_e . Therefore, during contact with soft environments, $\tau \approx \frac{ak_s + b'k_d}{b'k_s}$ and $k_{ap} \approx 0$; while for hard environments) $\tau \approx \frac{1}{\beta}$ and $k_{ap} \approx \frac{k_s}{\beta}$. Since the environmental stiffness k_e can vary by several orders of magnitude, if the compensator parameters $[\alpha, \beta, k_d, k_s]$ are fixed, the robot will exhibit highly non-uniform and possibly unstable response characteristics when contacting different environments.

In order to overcome this problem and obtain a uniform and desirable performance, a simple adaptive scheme is proposed to "tune" the compensator gains α and β automatically on-line as functions of the contact force F , while choosing constant values for k_d and k_s . In practice, we set $k_s = 1$ and choose k_d to filter out the force measurement noise. Suppose that the desired dynamic performance of the contact force F in response to the reference position x_r is described by the *target interaction dynamics*

$$\frac{\tau_m}{k_m} \dot{F}_m(t) + \frac{1}{k_m} F_m(t) = k_d \dot{x}_r(t) + k_s x_r(t) \quad (62)$$

or

$$\frac{F_m(s)}{x_r(s)} = \frac{k_m(k_d s + k_s)}{\tau_m s + 1} \quad (63)$$

where F_m denotes the desired behavior of F , and τ_m and k_m are the desired user-specified time-constant and apparent stiffness, respectively. This ensures that the environment behaves like a simple spring-damper-spring system with user-specified parameters τ_m, k_m, k_d , and k_s . Notice that the target dynamics (62)-(63) can be written as

$$\frac{\tau_m}{k_m} \frac{d}{dt} \hat{F}_m(t) + \frac{1}{k_m} \hat{F}_m(t) = \frac{F_r(s)}{x_r(s)} \frac{k_m}{\tau_m s + 1} \quad (64)$$

where \hat{F}_m is the desired behavior of the filtered force \hat{F} . Now, following Appendix IV, the adaptation laws for $\alpha(t)$ and $\beta(t)$ which ensure that the actual interaction dynamics (59) tends to the target interaction dynamics (62) are given by

$$\alpha(t) = \alpha(0) - \gamma_1 \int_0^t e(t) \dot{F}(t) dt - \gamma_2 e(t) \dot{F}(t) \quad (65)$$

$$\beta(t) = \beta(0) + \lambda_1 \int_0^t e(t) F(t) dt + \lambda_2 e(t) F(t) \quad (66)$$

where $e(t) = F(t) - F_m(t)$ is the deviation of the actual contact force $F(t)$ from its desired value $F_m(t)$, $[\gamma_1, \lambda_1]$ are constant positive integral adaptation gains, and $[-\gamma_2, \lambda_2]$ are zero or positive constant proportional adaptation gains. The adaptation laws (65)-(66) ensure that the actual contact force F follows the desired contact force F_m asymptotically, i.e., $e(t) \rightarrow 0$ as $t \rightarrow \infty$. Note that the desired force $F_m(t)$ is obtained by solving the target interaction dynamics (62) with the given reference position $x_r(t)$. To enhance robustness to the unmodeled manipulator dynamics, the σ -modification method [43] is used, and the improved adaptation laws are given by

$$\alpha(t) = \alpha(0) + \gamma_1 \int_0^t e(t) \dot{F}(t) dt + \gamma_2 e(t) \dot{F}(t) - \sigma_1 \int_0^t \alpha(t) dt \quad (67)$$

$$\beta(t) = \beta(0) + \lambda_1 \int_0^t e(t) F(t) dt + \lambda_2 e(t) F(t) - \sigma_2 \int_0^t \beta(t) dt \quad (68)$$

The σ -modified adaptation laws (67)-(68) for α and β ensure that the residual tracking-error $e = F - F_m$ tends to a bounded set of order (a) , while guaranteeing robustness to the unmodeled third and second-order dynamic terms in equation (58).

Finally, by setting $\gamma_2 = 0$ and using integration-by-parts, equation (67) simplifies to

$$\begin{aligned} \alpha(t) &= \alpha(0) + \gamma_1 \int_0^t [F'(t) - F_m'(t)] \dot{F}'(t) dt - \sigma_1 \int_0^t \alpha(t) dt \\ &= \alpha(0) + \frac{1}{2} \gamma_1 F'^2(t) - \gamma_1 F_m'(t) F'(t) + \gamma_1 \int_0^t \dot{F}_m'(t) F'(t) dt - \sigma_1 \int_0^t \alpha(t) dt \end{aligned} \quad (69)$$

Note that since the desired contact force $F_m'(t)$ is a smooth noise-free signal obtained from the target interaction model (62), the desired force rate $\dot{F}_m'(t)$ can be computed directly and used in the adaptation law (69). It is seen that the computation of the compensator gain $\alpha(t)$ from equation (69) does not require knowledge of the actual force rate $\dot{F}'(t)$, which can be difficult to obtain in practice since $F'(t)$ is a noisy signal.

We conclude that the adaptive lag-plus-feedforward compliance control law is given by

$$x_f(t) = \frac{1}{k_d} \alpha(t) F'(t) - 1 [\beta(t) \frac{k_s}{k_d} \alpha(t)] \hat{F}'(t) \quad (70)$$

where \hat{F}' is the filtered contact force, and the control scheme is shown in Figure 14. *Notice that neither the compliance control law (70) nor the adaptation laws (68)-(69) require the contact force rate information $\dot{F}'(t)$.*

6 Simulation Study

The force control schemes described in Sections 4 and 5 are now applied through computer simulations to the 7 DOF Robotics Research Corporation (RRC) Model K-1607 arm, shown in Figure 15. The complete kinematic and dynamic models for this arm are integrated into a graphics-based robot simulation environment hosted on a Silicon Graphics PersonalIRIS workstation [45]. The simulation software incorporates models of all important dynamic sub-systems and phenomena, such as full nonlinear arm dynamics, joint stiction, and transmission effects, and therefore provides the basis for a realistic evaluation of the control system performance. The RRC arm has an anthropomorphic design with seven revolute joints, and is one of the few commercially available kinematically redundant manipulators. The overall reach of the arm is approximately 80in and the total weight of the arm is over 500lb.

In the simulations, the robot position control system employs a high-performance adaptive controller described in [40]. This controller ensures that any commanded end-effector position trajectory x_c is tracked accurately. All integrations required by the force control schemes are implemented using a simple trapezoidal integration rule with a time-step of one millisecond. Throughout the simulations, the unit of length is inch, the unit of time is second, the unit of angle is degree, and the unit of force is pound.

The simulation study demonstrates the capability of the proposed admittance and compliance control schemes to achieve a desired end-effector/environment contact force. In this study, a frictionless reaction surface modeled as linearly elastic with a stiffness of 100lb./in in series with a uni-directional damper having the friction coefficient of 10lb.sec./in is placed in the robot workspace. This reaction surface is oriented normal to the y axis and is located at $y_e = -22.125$; thus the measured contact force F' is modeled as

$$F' = \begin{cases} 0 & \text{if } y \leq -22.125 & \text{(no contact)} \\ 100(y + 22.125) - 10\dot{y} & \text{if } y > -22.125 \text{ and } \dot{y} > 0 & \text{(contact, moving in)} \\ 100(y + 22.125) & \text{if } y > -22.125 \text{ and } \dot{y} \leq 0 & \text{(contact, moving out)} \end{cases}$$

The task requires the exertion of a 10lb contact force normal to the reaction surface while tracking a smooth 5in trajectory tangent to the surface. Thus we define $F_r' = 10$ and $x_r = x_i - 2.5[1 - \cos(\pi/5)t]$ for $t \in [0, 5]$, where x_i is the x component of the initial end-effector position. For simplicity, the end-effector orientation and z coordinate are maintained at their initial values throughout the task.

To illustrate robustness of the force control schemes in accommodating unexpected changes in the environmental stiffness, the stiffness k_e is changed abruptly from $k_e = 100\text{lb/in}$ to $k_e = 25\text{lb/in}$ at the midpoint of the x_r trajectory at $t = 2.5$ seconds. The control objective is to maintain the contact force at 10lb despite this stiffness variation. This situation can occur in practice when tracking along a surface composed of two materials with different stiffnesses.

Two computer simulation studies are now described using the explicit force control (admittance control) and the implicit force control (compliance control) schemes developed in Sections 4 and 5.

G. 1 Adaptive Admittance Control

In this case, we use the adaptive PI force control law

$$y_f(t) = [k_{p0} + \alpha e^2(t)]e(t) + k_i \int_0^t e(t)dt \quad (71)$$

developed in Section 4.2, where $e = F_r' - F'$ is the force tracking-error. This control scheme has the attractive feature of *not* requiring force rate information for implementation. The desired force setpoint is specified as

$$F_r'(t) = \begin{cases} 5[1 - \cos \pi t] & t < 1 \\ 10 & t \geq 1 \end{cases}$$

so that the force setpoint changes smoothly from 0 to 10lb in 1 second.

First, the open-loop response of the contact force F' to the step reference input y_r with no force feedback ($y_f = 0$) is obtained. The response indicates that the robot-plus-position controller-plus-reaction surface can be approximated by a linear second-order transfer-function

with) the forward path gain $\frac{bk_e}{y} = 100$ and the attenuation factor $a = 10$, since for the command $y_r = 0.2$ inches the force response reaches the steady-state value $F'_{ss} = 20$ lb in 1 second. Following Section 4.2, the integral gain k_i and the initial proportional gain k_{p0} are chosen as $k_i = 0.10$ and $k_{p0} = 0.004$ to satisfy the inequality $0 < k_i < a [k_{p0}^{-1} \&]$. The rate-of-adaptation of the proportional gain is chosen as $\alpha = 0.0001$ and the reference position is set to $y_r = 0.2$ inches. Figures 16a and 16b show the variations of the contact force F' and the adaptive proportions] gain k_p during the task. From Figure 16a, it is seen that F' tracks the desired force setpoint F'_r in the steady-state, which is reached in 1 second. The contact force is then perturbed at $t = 2.5$ seconds due to the change in environmental stiffness, but recovers subsequently due to the integral action to, settle again at the desired setpoint $F'_r = 10$ lb in the steady-state. Figure 16b shows that the adaptive term $\alpha e^2(t)$ in the proportional gain k_p causes an increase in the value of k_p during the transient responses, where there are discrepancies between the actual and desired forces. Once the force tracking-error e diminishes to zero in the steady-state, the proportional gain returns to its initial value k_{p0} . Hence, the compensator adaptation improves the transient behavior by increasing k_p automatically when e is large, without affecting the steady-state performance.

6.2 Adaptive Compliance Control

in this case, we use the MILAC-based adaptive lag-plus-feedforward compliance compensator $K(s) = \frac{\alpha s + \beta}{k_d s + k_s}$ developed in Section 5.3, where α and β are adaptive gains while k_d and k_s are fixed coefficients set at $k_d = 0.05$, and $k_s = 1$. With this choice of (k_d, k_s) , the cutoff frequency of the low-pass filter $\frac{1}{k_d s + k_s}$ is at 20 rad/sec. For compliance control, there is no force setpoint F'_r ; instead the desired contact dynamics is specified by the user. Suppose that the target contact dynamics is chosen as

$$0.004 \dot{F}'_m(t) - 10.02 F'_m(t) = 0.05 \dot{y}_r(t) - y_r(t) \quad (72)$$

which has the desired time-constant $\tau_m = \frac{0.004}{0.02} = 0.2$ sec and the desired stiffness $k_m = \frac{1}{0.02} = 50$ b/in. To obtain a constant contact force of 10 lb, the reference position is chosen to penetrate into the reaction surface by $y_r = 0.2$ inches, so that $F'_{ss} = k_m y_r = (50)(0.2) = 10$ lb. The adaptation laws for the compensator gains α and β are chosen as

$$\begin{aligned} \alpha(t) &= 10^{-4} \left\{ 0.1 - 10.001 \int_0^t e(t) \dot{F}'(t) dt - \int_0^t \alpha(t) dt \right\} \\ \beta(t) &= 10^{-4} \left\{ 0.1 - 10 \int_0^t e(t) F'(t) dt - \int_0^t \beta(t) dt \right\} \end{aligned} \quad (73)$$

where $e(t) = F'(t) - F'_m(t)$, and $F'_m(t)$ is obtained by solving the target dynamics (72) with $y_r = 0.2$. Figures 17a and 17b depict the variations of the contact force F' and the compensator gain β during the task. From Figure 17a, it is seen that initially the contact

Since the adaptation gain for α is small, α varies very slightly from its initial value.

force F responds rapidly to the step reference position y_r . This initial deviation of F from F_m causes the adaptive gain β to increase, which in turn forces F to track the desired trajectory F_m . The transient response lasts $5\tau_m = 1$ second and for $t > 1$, F tracks F_m exactly and reaches the steady-state value $F_{ss} = k_m y_r = 10$ lb. At $t = 2.5$ sec when the environmental stiffness k_e decreases abruptly, the contact force drops instantaneously but is restored to the target force F_m in 1.5 seconds. Since β determines the stiffness of the compensator as given by $k_c = K'(0) = \frac{k_s}{\beta} = \beta^{-1}$, it is interesting to consider the steady-state values of β in the time periods $0 < t < 2.5$ and $2.5 < t < 5$. During contact with the hard surface ($k_e = 100$), from Figure 17b we have $\beta_{ss} = 0.01$; hence $k_c = 100$ and the apparent stiffness is $k_{ap} = [k_c^{-1} + k_e^{-1}]^{-1} = [0.01^{-1} + 0.01^{-1}]^{-1} = 50$ which is the specified model stiffness k_m . During contact with the soft surface ($k_e = 25$), from Figure 17b we have $\beta_{ss} = -0.02$; hence $k_c = -50$ and $k_{ap} = [-0.02^{-1} + 0.04^{-1}]^{-1} = 50 = k_m$ again. We conclude that the adaptation law has resulted in a *negative* value for β [corresponding to positive force feedback loop] in order to increase the apparent stiffness of the surface from $k_e = 25$ to $k_m = 50$. Finally, note that from Section 5.3 the force rate information \dot{F} is *not* required for implementation of this control scheme.

7 Discussions and Conclusions

Two classes of force control schemes based on compliant motion are discussed in this paper. The admittance control approach is an explicit force control scheme that uses force setpoint as command and accomplishes contact force control directly. The compliance control approach, on the other hand, is an implicit force control scheme that uses reference position as command and achieves a desired contact dynamics. Both schemes use adaptive compensator gains to ensure stable and uniform performance in contact with environments having unknown stiffnesses.

It is interesting to compare the performance of admittance and compliance control schemes for constrained tasks. The admittance scheme has the advantage of robust force setpoint tracking and rejection of constant disturbances. However, it has the disadvantage of requiring switching between x_r as command (for unconstrained tasks) and F_r as command (for constrained tasks), and possibly poor transition response. The compliance scheme, on the other hand, has the advantage of not switching commands between unconstrained and constrained tasks (both with x_r as command), and therefore generally good response at transition. However, it has the disadvantage of possibly less robust command tracking and disturbance rejection. Therefore, the utilization of admittance or compliance control is dictated by the requirements of the particular application at hand.

Finally, it is important to appreciate the subtle difference between the conventional impedance control and the proposed compliance control. Consider the standard second-order target impedance dynamics [3]

$$m\ddot{x}_r + b[\dot{x}_r - \dot{x}] + k[x_r - x] = F \quad (74)$$

where x_r is the reference position and x is the actual position of the end-effector and F is the contact force. Assuming a linearly elastic environment, $F = k_e x$, equation (74) reduces to

$$\frac{b}{k_e} \dot{F} + \left(1 + \frac{k}{k_e}\right) F = m\ddot{x}_r + b\dot{x}_r + kx_r \quad (75)$$

It is seen that the dynamic model relating x_r to F is dependent on the environmental stiffness k_e . Hence, under impedance control, the robot will exhibit different characteristics, e.g., apparent stiffness and response time, when contacting different environments. This is in contrast to the proposed compliance control approach which attempts to maintain a user-specified invariant target dynamics between x_r and F irrespective of the environmental stiffness, such as

$$\frac{\tau_m}{k_m} \dot{F}_m(t) + \frac{1}{k_n} F_m(t) = k_d \dot{x}_r(t) + k_s x_r(t) \quad (76)$$

where τ_m , k_m , k_d , and k_s are user-specified parameters. Hence, the goal of compliance control is to provide the same robot-environment interaction dynamics regardless of the environmental stiffness.

The analysis presented in Sections 4 and 5 is in continuous-time and predicts closed-loop stability for arbitrary large environmental stiffness or compensator gain. However, in performing the computer simulations of Section 6, it was found that the force control system tends to become unstable when the environmental stiffness or the compensator gain have large numerical values. This instability can be attributed to the discretization effects (such as zero-order hold, sampling, etc.) present in the discrete-time implementation of the force control schemes. In discrete-time control systems, decreasing the sampling period T results in an increase in the range of allowable loop gain k and yields improved system performance; while increasing T will require a decrease in k and results in degradation of system performance [see, e.g., 1]. As a consequence, simple force control laws that can be computed rapidly, such as those developed in Sections 4 and 5, allow a smaller sampling period to be used and lead to more stable closed-loop force control systems.

Current work is aimed at real-time implementation and experimental evaluation of the admittance and compliance control schemes proposed in this paper on a 7 DOF Robotics Research arm. Proper utilization of the arm redundancy to improve the system performance will also be investigated.

8 Appendices

In these Appendices, we derive the results used in the development of the admittance and compliance control schemes in Sections 4 and 5.

8.1 Appendix 1: Derivation of Adaptation Laws for Admittance Control

Consider the second-order system

$$\ddot{e}(t) - a(t)\dot{e}(t) - b(t)e(t) = f(t) \quad (77)$$

where $a(t)$, $b(t)$ and $f(t)$ contain both fixed system parameters and adjustable controller gains. Let the desired behavior of $e(t)$ be described by the second-order reference model

$$\ddot{e}_m(t) - 2\zeta\omega\dot{e}_m(t) - \omega^2 e_m(t) = 0 \quad (78)$$

where ζ and ω are the user-specified clamping ratio and undamped natural frequency, respectively. The problem is to find the appropriate time functions $[a(t), b(t), f(t)]$ such that the state of the adjustable system (77), i.e., $\begin{bmatrix} e(t) \\ \dot{e}(t) \end{bmatrix}$, tends to that of the reference model (78), i.e., $\begin{bmatrix} e_m(t) \\ \dot{e}_m(t) \end{bmatrix}$, asymptotically. To this end, we subtract equation (78) from equation (77) to obtain

$$(e - e_m) - 2\zeta\omega(\dot{e} - \dot{e}_m) - \omega^2(e - e_m) = f - (2\zeta\omega - a)\dot{e} + (\omega^2 - b)e$$

or, in the state-space form

$$\dot{E} = \begin{pmatrix} 0 & 1 \\ -\omega^2 & -2\zeta\omega \end{pmatrix} E + \begin{pmatrix} 0 \\ \omega^2 - b - 2\zeta\omega - a \end{pmatrix} \begin{pmatrix} e \\ \dot{e} \end{pmatrix} + \begin{pmatrix} 0 \\ f \end{pmatrix} \quad (79)$$

Where $E = [(e - e_m), (\dot{e} - \dot{e}_m)]^T$ is the 2x1 tracking-error vector. Let us define the positive scalar Lyapunov function candidate

$$V = E^T P E + Q_0 (f - f^*)^2 + Q_1 (\omega^2 - b + b^*)^2 + Q_2 (2\zeta\omega - a + a^*)^2 \quad (80)$$

where $[f^*, b^*, a^*]$ are functions of time to be specified later, $[Q_0, Q_1, Q_2]$ are constant positive scalars, and $P = \begin{pmatrix} p_1 & p_2 \\ p_2 & p_3 \end{pmatrix}$ is the 2x2 constant symmetric positive-definite matrix which satisfies the Lyapunov equation for the reference model, i.e.,

$$\begin{pmatrix} p_1 & p_2 \\ p_2 & p_3 \end{pmatrix} \begin{pmatrix} 0 & 1 \\ -\omega^2 & -2\zeta\omega \end{pmatrix} + \begin{pmatrix} 0 & -\omega^2 \\ 1 & -2\zeta\omega \end{pmatrix} \begin{pmatrix} p_1 & p_2 \\ p_2 & p_3 \end{pmatrix} = - \begin{pmatrix} q_1 & q_2 \\ q_2 & q_3 \end{pmatrix} \quad (81)$$

where $Q = \begin{pmatrix} q_1 & q_2 \\ q_2 & q_3 \end{pmatrix}$ is a symmetric positive-definite 2x2 matrix. Differentiating V along the error trajectory (79) and simplifying the result, we obtain

$$\begin{aligned} \dot{V} = & -E^T Q E - [2Q_0 f(\dot{f} - \dot{f}^*) - 2q_j - 2Q_0 f^*(\dot{f} - \dot{f}^*)] \\ & + [2Q_1 (b - \omega^2)(\dot{b} - \dot{b}^*) - 2q(b - \omega^2)e - 2Q_1 b^*(\dot{b} - \dot{b}^*)] \\ & - [2Q_2 (a - 2\zeta\omega)(\dot{a} - \dot{a}^*) - 2q(a - 2\zeta\omega)\dot{e} - 2Q_2 a^*(\dot{a} - \dot{a}^*)] \end{aligned} \quad (82)$$

where $q = p_2 c + p_3 \dot{e}$ is the weighted position-velocity error. To ensure asymptotic stability of (79), we set

$$\begin{aligned}
2Q_0 f(\dot{j} - \dot{j}^*) - 2q\dot{f} = 0 &\rightarrow \dot{j} - \dot{\mathbf{f}}^* = \frac{-1}{Q_0} q \\
2Q_1 (b - \omega^2)(\dot{b} - \dot{b}^*) - 2q(b - \omega^2)e = 0 &\rightarrow b - b^* = \frac{1}{Q_1} qe \\
2Q_2 (a - 2\zeta\omega)(\dot{a} - \dot{a}^*) - 2q(a - 2\zeta\omega)\dot{e} = 0 &\rightarrow \dot{a} - \dot{a}^* = \frac{1}{Q_2} q\dot{e}
\end{aligned} \tag{83}$$

in this case, we obtain

$$\mathbf{V} = -\dot{\mathbf{f}}^T Q \dot{\mathbf{E}} - 2j^* \dot{q} - 2b^* q \dot{e} - 2a^* q \dot{e}$$

Now, let us choose j^* , u^* , b^* as follows:

$$\begin{aligned}
j^* &= -Q_0^* q \\
b^* &= Q_1^* qe \\
a^* &= Q_2^* q\dot{e}
\end{aligned} \tag{84}$$

where Q_0^* , Q_1^* , Q_2^* are zero or positive constants. Then, $\dot{\mathbf{V}}$ simplifies to

$$\dot{\mathbf{V}} = -\dot{\mathbf{f}}^T Q \dot{\mathbf{E}} - 2Q_0^* q^2 - 2Q_1^* (qe)^2 - 2Q_2^* (q\dot{e})^2 \tag{85}$$

which is negative-definite in $\dot{\mathbf{E}}$, and hence (79) is stable [46]. From (83) and (84), the adaptation laws for j , a , and b are obtained as

$$\begin{aligned}
\dot{j} &= \frac{-1}{Q_0} q - Q_0^* \frac{d}{dt}[q] \\
\dot{b} &= \frac{1}{Q_1} qe + Q_1^* \frac{d}{dt}[qe] \\
\dot{a} &= \frac{1}{Q_2} q\dot{e} + Q_2^* \frac{d}{dt}[q\dot{e}]
\end{aligned} \tag{86}$$

and hence

$$\begin{aligned}
f(t) &= f(0) - \frac{1}{Q_0} \int_0^t q(t) dt - Q_0^* q(t) \\
b(t) &= b(0) + \frac{1}{Q_1} \int_0^t q(t)e(t) dt + Q_1^* q(t)e(t) \\
a(t) &= a(0) + \frac{1}{Q_2} \int_0^t q(t)\dot{e}(t) dt + Q_2^* q(t)\dot{e}(t)
\end{aligned} \tag{87}$$

where

$$q(t) = w_p e(t) + w_d \dot{e}(t)$$

and $w_p = p_2$, $w_d = p_3$. A closer look at (87) reveals that

$$f(t) = j(0) - \left[w_p Q_0^* + \frac{w_d}{Q_0} \right] e(t) - \frac{w_p}{Q_0} \int_0^t e(t) dt - [w_d Q_0^*] \dot{e}(t) \tag{88}$$

which shows that the auxiliary signal $f(t)$ is produced by a *constant-gain* PID controller acting on the error $e(t)$. Note that $f(t)$, $a(t)$, and $b(t)$ vary as functions of $e(t)$ and $\dot{e}(t)$ until $e = \dot{e} = 0$ in which case j , a , and b reach constant values.

8.2 Appendix 11: Barbashin's Theorem for Third-Order Nonlinear Systems

Recall the error differential equation (24) in Section 4.2, viz:

$$\ddot{e} + a\dot{e} + [b' + bk_e k_p]e + bk_e k_i \int_0^t e dt = b'[I_r - I_x] \quad (89)$$

Let us define new variables as follows:

$$\begin{aligned} x_1 &= \int_0^t e dt - C \\ x_2 &= \dot{x}_1 = e \\ x_3 &= \dot{x}_2 = \dot{e} \end{aligned}$$

where $c = \frac{b'}{bk_e k_i} [I_r - I_x]$ is a constant. Then (89) can be written as the homogeneous equation

$$\ddot{x}_1 - a\dot{x}_1 - [b' - bk_e k_p]\dot{x}_1 + bk_e k_i x_1 = 0 \quad (90)$$

Specific stability criteria have been obtained for one particular class of third-order systems by Barbashin [44]. The system is described by the state equations

$$\begin{aligned} \dot{x}_1 &= x_2 \\ \dot{x}_2 &= x_3 \\ \dot{x}_3 &= -f(x_1) - g(x_2) - ax_3 \end{aligned} \quad (91)$$

where $j(0) = 0$ and $g(0) = 0$, and both $f(x_1)$ and $g(x_2)$ are differentiable. If written as a single third-order differential equation, this system is equivalent to

$$\ddot{x}_1 - a\dot{x}_1 - g(\dot{x}_1) - f(x_1) = 0 \quad (92)$$

The equilibrium point, $x_e = 0$, is asymptotically stable in the large if

$$\begin{aligned} \text{(i)} \quad & a > 0 \\ \text{(ii)} \quad & f(x_1)x_1 > 0, \quad x_1 \neq 0 \\ \text{(iii)} \quad & ag(x_2)/x_2 - f'(x_1) > 0, \quad x_2 \neq 0 \end{aligned} \quad (93)$$

where $f'(x_1) = d[f(x_1)]/dx_1$. Note that in terms of the original variables, the equilibrium point is defined as $\{\int_0^t e dt = c, e = 0, \dot{e} = 0\}$. While equations (91) and (92) are written with dots indicating differentiation with respect to time, the independent variable must be a dimensionless time in order that the x 's be of the same dimensions and the criteria of equation (93) be directly applicable. A scalar Lyapunov function for the system is

$$v(x) = aF(x_1) + f(x_1)x_2 - G(x_2) + 1/2(ax_2 - x_3)^2 \quad (94)$$

where $F(x_1) = \int_0^{x_1} f(x_1)dx_1$ and $G(x_2) = \int_0^{x_2} g(x_2)dx_2$. Then, we obtain

$$v(x) = - [ag(x_2)/x_2 - f'(x_1)]x_2^2 \quad (95)$$

Thus, provided that the conditions of equations (93) apply, then $V(x) > 0$ and $\dot{V}(x) < 0$, and therefore the system is asymptotically stable. Note that the variable x_3 does not appear in $\dot{V}(x)$.

While equation (92) is a nonlinear third-order equation with rather general nonlinearities allowed in both the dependent variable x_1 and its first derivative \dot{x}_1 , it is necessary that there be no products of these two types of terms, and that the second and third derivatives appear only in linear terms. Note that for the linear third-order differential equations

$$\ddot{x}_1 + a_1 \dot{x}_1 + a_2 x_1 = a_3 x_1 \quad (95)$$

where a_1 , a_2 , and a_3 are positive constants, Lyapunov's Theorem reduces to the classical Routh-Hurwitz condition, namely

$$a_1 a_2 > a_3$$

8.3 Appendix III: Boundedness of $\beta + F \frac{d\beta}{dF}$ in Compliance Control

In this Appendix, we show that using the adaptive compensator gain

$$\beta = \beta_0 + \gamma [1 - \exp(F_m - F)/\tau] \quad (96)$$

the expression

$$A = \beta + F \frac{d\beta}{dF} \quad (97)$$

is upper bounded. Using equation (96), A can be expressed as

$$A = \beta_0 - \gamma + \gamma(F/\tau - 1) \exp(F_m - F)/\tau = \beta_0 - \gamma + \gamma B \quad (98)$$

where $B = (F/\tau - 1) \exp(F_m - F)/\tau$. To determine the extremum of B as a function of F , we find

$$\frac{dB}{dF} = \frac{1}{\tau} (2 - F/\tau) \exp(F_m - F)/\tau = 0 \quad (99)$$

hence $\{F = 2\tau, B = \exp(F_m/\tau - 2)\}$ defines the maximum of B . Therefore, B starts at $-\exp(F_m/\tau)$ for $F = 0$, increases to $\exp(F_m/\tau - 2)$ as F increases from 0 to 2τ , and then decreases to zero as F tends to infinity. Thus B is bounded by

$$-\exp(F_m/\tau) \leq B \leq \exp(F_m/\tau - 2)$$

We conclude that the upper bound on A is

$$A \leq \beta_m \quad (100)$$

where $\beta_m = \beta_0 - \gamma [1 + \exp(F_m/\tau - 2)]$.

8.4 Appendix IV: Derivation of Adaptation Laws for Compliance Control

Consider the first-order *adjustable system*

$$a(t)\dot{x}(t) + b(t)x(t) = u(t) \quad (101)$$

where $u(t)$ is the scalar input, $x(t)$ is the scalar output, and the coefficients $a(t)$ and $b(t)$ contain both fixed system parameters and adjustable controller gains. Let the desired behavior of the output $x_r(t)$ be described by the first-order *reference model*

$$a_m \dot{x}_m(t) + b_m x_m(t) = u(t) \quad (102)$$

where a_m and b_m are positive constant coefficients chosen by the user to ensure that x_m responds to u with a desirable time-constant $\tau = \frac{a_m}{b_m}$ and steady-state gain $k = \frac{1}{b_m}$, that is, $\frac{x_m(s)}{u(s)} = \frac{1}{b_m + a_m s} = \frac{k}{1 + \tau s}$. The problem is to find the appropriate time functions $[a(t), b(t)]$ such that, for all inputs $u(t)$, the output $x(t)$ of the adjustable system (101) tends to the output $x_m(t)$ of the reference model (102) asymptotically; i.e., $x(t) \rightarrow x_m(t)$ as $t \rightarrow \infty$. To this end, we subtract equation (102) from equation (101) to obtain, after some simplification, the error differential equation

$$\dot{e}(t) = -\frac{b_m}{a_m} e(t) - \frac{b_m - b(t)}{a_m} x(t) - \frac{a_m - a(t)}{a_m} \dot{x}(t) \quad (103)$$

Where $e(t) = x(t) - x_m(t)$ is the output tracking-error. Let us define the positive scalar Lyapunov function candidate

$$V(t) = q_0 e^2(t) + q_1 \left[\frac{b_m - b(t)}{a_m} x(t) \right]^2 + q_2 \left[\frac{a_m - a(t)}{a_m} \dot{x}(t) \right]^2 \quad (104)$$

where $[q_1^*(t), q_2(t)]$ are time functions to be specified later, and $[q_0, q_1, q_2]$ are constant positive scalars. Differentiating $V(t)$ with respect to time along the error trajectory (103) and simplifying the result, we obtain

$$\begin{aligned} \dot{V} = & -2 \frac{b_m}{a_m} q_0 e^2 - 2 \left[\left(\frac{b_m - b}{a_m} \right) \left(q_0 e \dot{x} - \frac{q_1 \dot{b}}{a_m} x - q_1 \dot{q}_1^* \right) + q_1 q_1^* \left(\frac{\dot{b}}{a_m} + \dots \right) \right. \\ & \left. - 2 \left[\left(\frac{q_2 \dot{a}}{a_m} - q_2 \dot{q}_2^* \right) + q_2 q_2^* \left(\frac{\dot{a}}{a_m} + \dot{q}_2^* \right) \right] \right] \quad (105) \end{aligned}$$

To ensure asymptotic stability of the error differential equation (103), we set

$$\begin{aligned} q_0 e \dot{x} - \frac{q_1 \dot{b}}{a_m} x - q_1 \dot{q}_1^* = 0 & \rightarrow \frac{\dot{b}}{a_m} + \dot{q}_1^* = \frac{q_0}{q_1} e \dot{x} \\ q_0 e \dot{x} - \frac{q_2 \dot{a}}{a_m} - q_2 \dot{q}_2^* = 0 & \rightarrow \frac{\dot{a}}{a_m} + \dot{q}_2^* = \frac{q_0}{q_2} e \dot{x} \end{aligned} \quad (106)$$

Using equation (106), V in equation (105) simplifies to

$$\dot{V} = -2\frac{b_m}{a_m} q_0 e^2 + 2q_1^* q_0 e x + 2q_2^* q_0 e \dot{x}$$

Now, let us choose q_1^*, q_2^* as follows:

$$q_1^* = -p_1 e x \quad (107)$$

$$q_2^* = -p_2 e \dot{x}$$

where p_1 and p_2 are zero or positive constants. Then, V simplifies to

$$V = -2\frac{b_m}{a_m} q_0 e^2 - 2p_1 q_0 (e x)^2 - 2p_2 q_0 (e \dot{x})^2$$

which is negative-definite in e , and hence (103) is stable [46]. From (106) and (107), the adaptation laws for a and b are obtained as

$$\dot{b} = a_m \frac{q_0}{q_1} e x - a_m \dot{q}_1^* = a_m \frac{q_0}{q_1} e x + a_m p_1 \frac{d}{dt} (e x) \quad (108)$$

$$\dot{a} = a_m \frac{q_0}{q_2} e \dot{x} - a_m \dot{q}_2^* = a_m \frac{q_0}{q_2} e \dot{x} + a_m p_2 \frac{d}{dt} (e \dot{x}) \quad (109)$$

Let us define the adaptation gains

$$\gamma_1 = a_m \frac{q_0}{q_1} ; \quad \gamma_2 = a_m p_1$$

$$\lambda_1 = a_m \frac{q_0}{q_2} ; \quad \lambda_2 = a_m p_2$$

and integrate equations (108) and (109) to yield

$$b(t) = b(0) + \gamma_1 \int_0^t e(t) x(t) dt + \gamma_2 e(t) x(t) \quad (110)$$

$$a(t) = a(0) + \lambda_1 \int_0^t e(t) \dot{x}(t) dt + \lambda_2 e(t) \dot{x}(t) \quad (111)$$

Note that $a(t)$ and $b(t)$ vary as functions of $e(t)$ until $e(t) = 0$; i.e., $x(t) = x_m(t)$, in which case a and b reach constant values.

9 Acknowledgments

The research described in this paper was carried out at the Jet I 'repulsion laboratory, California Institute of Technology, under contract with the National Aeronautics and Space Administration. Fruitful discussions with Richard Colbaugh of New Mexico State University are gratefully acknowledged.

References

- [1] D.D. Whitney: "Force Feedback Control of Manipulator Fine Motions," ASME Journal of Dynamic Systems, Measurement, and Control, pp. 91-97, 1977.
- [2] M. Raibert and J. Craig: "Hybrid Position/Force Control of Manipulators", ASME Journal of Dynamic Systems, Measurement, and Control, Vol. 102, No. 2, pp. 126-133, 1981.
- [3] N. Hogan: "Impedance Control: An Approach to Manipulation, Parts I-III", ASME Journal of Dynamic Systems, Measurement, and Control, Vol. 107, No. 1, pp. 1-24, 1985.
- [4] H. Kazerooni, J. B. Sheridan, and P. K. Houpt: "Robust Compliant Motion for Manipulators, Parts I-III", IEEE Journal of Robotics and Automation, Vol. RA-2, No. 2, pp. 83-105, 1986.
- [5] H. Kazerooni: "On the Robot Compliant Motion Control," ASME Journal of Dynamic Systems, Measurement and Control, Vol. 111, pp. 416-425, 1989.
- [6] H. Kazerooni: "Compliant Motion Control for Robot Manipulators," International Journal of Control, Vol. 49, No. 3, pp. 745-760, 1989.
- [7] H. Kazerooni, B. J. Waibel, and S. Kim: "On the Stability of Robot Compliant Motion Control," ASME Journal of Dynamic Systems, Measurement, and Control, Vol. 112, pp. 417-426, 1990.
- [8] H. Kazerooni, K. G. Bouklas, and J. Guo: "Theory and Experiments on the Compliance Control of Redundant Robot Manipulators," ASME Journal of Dynamic Systems, Measurement, and Control, Vol. 112, pp. 653-660, 1990.
- [9] B. J. Waibel and H. Kazerooni: "Theory and Experiments on the Stability of Robot Compliance Control," IEEE Transactions on Robotics and Automation, Vol. 7, No. 1, pp. 95-104, 1991.
- [10] D. A. Lawrence and R. M. Stoughton: "Position-Based Impedance Control: Achieving Stability in Practice," Proc. AIAA Guidance, Navigation, and Control Conference, pp. 221-226, Monterey, 1987.
- [11] J. D. Chapel and D. A. Lawrence: "Stability Analysis for Alternative Force Control Schemes as Applied to Remote Space Teleoperation," Proc. 10th Annual AAS Guidance and Control Conference, Keystone, 1987.
- [12] D. A. Lawrence: "Actuator limitations on Achievable Manipulator Impedance," Proc. IEEE International Conference on Robotics and Automation, pp. 560-565, Scottsdale, 1989.

- [13] D. A. Lawrence: "impedance Control Stability Properties in Common Implementations," Proc. IEEE International Conference on Robotics and Automation, pp. 1185-1190, Philadelphia, 1988.
- [14] D.F. Whitney: "Historical Perspective and State of the Art in Robot Force Control," international Journal of Robotics Research, Vol.6, No.1, pp. 3-14, 1987.
- [15] N. Hogan: "Stable Execution of Contact Tasks Using Impedance Control," Proc. IEEE International Conference on Robotics and Automation, pp.1047-1054, Raleigh, 1987.
- [16] N. Hogan: "On the Stability of Manipulators Performing Contact Tasks," IEEE Journal of Robotics and Automation, Vol. 4, No. 6, pp. 677-686, 1988.
- [17] J. K. Salisbury: "Active Stiffness Control of a Manipulator in Cartesian Coordinates," Proc. IEEE Conference on Decision and Control, pp. 93-98, Albuquerque, 1980.
- [18] W. S. Newman: "Stability and Performance Limits of interaction Controllers," ASME Journal of Dynamic Systems, Measurement, and Control, Vol. 114, pp. 563-570, 1992.
- [19] H. Ishikawa, C. Sawada, K. Kawase, and M. Takata: "Stable Compliance Control and its Implementation for a 6 DOF Manipulator," Proc. IEEE International Conference on Robotics and Automation, pp. 98-103, Scottsdale, 1989.
- [20] W. S. Kim, B. Hannaford, and A. K. Bejczy: "Force-Reflection and Shared Compliant Control in Operating Telemanipulators with Time Delay," IEEE Transactions on Robotics and Automation, Vol. 8, No. 2., pp. 176-185, 1992.
- [21] S. Lee and H.S. Lee: "Intelligent Control of Manipulators Interacting with an Uncertain Environment Based on Generalized Impedance," Proc. international Symposium on Intelligent Control, pp. 61-66, 1991.
- [22] Y. Xu, D. Ma, and J. M. Hollerbach: "Nonlinear Proportional and Derivative Control for High disturbance Rejection and High Gain Force Control," Proc. IEEE International Conference on Robotics and Automation, pp. 752-759, Atlanta, 1993.
- [23] J. P. Wen and S. H. Murphy: "Stability Analysis of Position and Force Control for Robotic Arms," IEEE Transactions on Automatic Control, Vol. 36, No. 3, pp. 365-371, 1991.
- [24] L. S. Wilfinger, J. P. Wen, and S. Murphy: "Integral Force Control with Robustness Enhancement," Proc. IEEE International Conference on Robotics and Automation, Vol. 1, pp. 100-105, Atlanta, 1993.
- [25] P. G. Backes: "Multi-Sensor Based Impedance Control for Task Execution," Proc. IEEE international Conference on Robotics and Automation, Vol. 2, pp. 1245-1250, Nice, France, 1992.

- [26] M. Pelletier and I. Daneshmand: "An Adaptive Compliant Motion Controller for Robot Manipulators Based on Damping Control", Proc. IEEE International Conference on Robotics and Automation, pp.78-83, Cincinnati, 1990.
- [27] P. Lasky and T. Hsia: "On Force-Tracking Impedance Control of Robot Manipulators", Proc. IEEE International Conference on Robotics and Automation, pp. 274-280, Sacramento, 1991.
- [28] S. Chan, B. Yao, W. Gao, and M. Cheng: "Robust Impedance Control of Robot Manipulators", International Journal of Robotics and Automation, Vol. 6, No. 4, pp. 220-227, 1991.
- [29] R. Anderson and M. Spong: "Hybrid Impedance Control of Robotic Manipulators," IEEE Journal of Robotics and Automation, Vol. 4, No. 5, pp. 549-555, 1988.
- [30] A. Goldenberg: "Implementation of Force and Impedance Control in Robot Manipulators," Proc. IEEE International Conference on Robotics and Automation, pp. 1626-1632, Philadelphia, 1988.
- [31] G. Niemeyer and J. J. Slotine: "Computational Algorithms for Adaptive Compliant Motion," Proc. IEEE International Conference on Robotics and Automation, pp. 566-571, Scottsdale, 1989.
- [32] R. Kelly, R. Carelli, M. Amestregus, and R. Ortega: "On Adaptive Impedance Control of Robot Manipulators," Proc. IEEE International Conference on Robotics and Automation, pp. 572-577, Scottsdale, 1989.
- [33] T. Tarn, A. Bejczy, and X. Yun: "Robot Arm Force Control through System Linearization by Nonlinear Feedback," Proc. IEEE International Conference on Robotics and Automation, pp. 1618-1625, Philadelphia, 1988.
- [34] O. Khatib: "A Unified Approach for Motion and Force Control of Robot Manipulators: The Operational Space Formulation," IEEE Journal of Robotics and Automation, Vol. 3, No. 1, pp.43-53, 1987.
- [35] O. Khatib and J. Burdick: "Motion and Force Control of Robot Manipulators," Proc. IEEE International Conference on Robotics and Automation, Vol. 3, pp. 1381-1386, San Francisco, 1986.
- [36] R. A. Volpe: "Real and Artificial Forces in the Control of Manipulators: Theory and Experiments," Ph.D. dissertation, Carnegie-MeHon University, 1990.
- [37] R. J. Anderson: "Dynamic Damping Control: Implementation Issues and Simulation Results," Proc. IEEE International Conference on Robotics and Automation, Vol, 1, pp. 68-77, Cincinnati, 1990.

- [38] S. D. Eppinger and W. P. Seering: "On Dynamic Models of Robot Force Control," Proc. IEEE International Conference on Robotics and Automation, Vol. 1, pp. 29-34, San Francisco, 1986.
- [39] H. Seraji: "Adaptive Force and Position Control of Manipulators," Journal of Robotic Systems, Vol. 4, No. 4, pp. 551-578, 1987.
- [40] R. Colbaugh, H. Seraji, and K. Glass: "Direct Adaptive Impedance Control of Robot Manipulators," Journal of Robotic Systems, Vol. 10, No. 2, pp. 217-224, 1993.
- [41] H. Seraji and R. Colbaugh: "Force Tracking in Impedance Control," Proc. IEEE International Conference on Robotics and Automation, Vol. 2, pp. 499-506, Atlanta, 1993.
- [42] M. C. Good, L. M. Sweet, and K. L. Strobel: "Dynamic Models for Control System Design of Integrated Robot and Drive Systems," ASME Journal, of Dynamic Systems, Measurement, and Control, Vol. 107, pp. 53-59, 1985.
- [43] P. A. Ioannou and P. V. Kokotovic: *Adaptive Systems with Reduced Models*, Springer-Verlag, New York, 1983.
- [44] W. J. Cunningham: "An Introduction to Lyapunov's Second Method," in 'Work Sessions in Lyapunov's Second Method,' L. F. Kazda (Ed.), 1960.
- [45] K. Glass and R. Colbaugh, "A Computer Simulation Environment for Manipulator Controller Development," NMSU Internal Publication, 1992.
- [46] K. Narendra and A. Annaswamy, *Stable Adaptive Systems*, Prentice Hall, Englewood Cliffs, NJ, 1989.

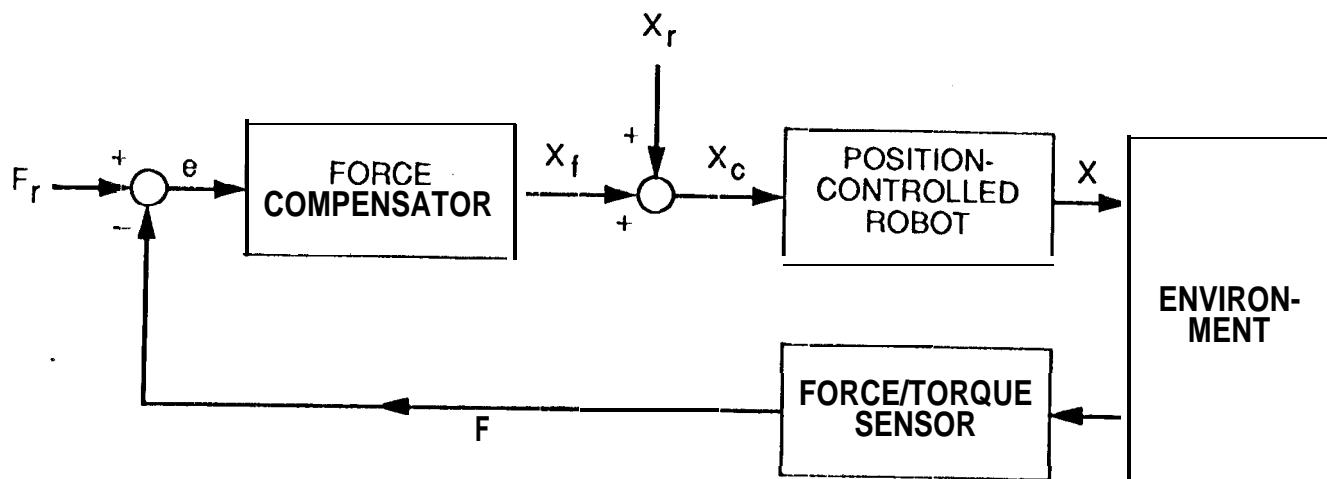


Figure 1. Position-based explicit force control system

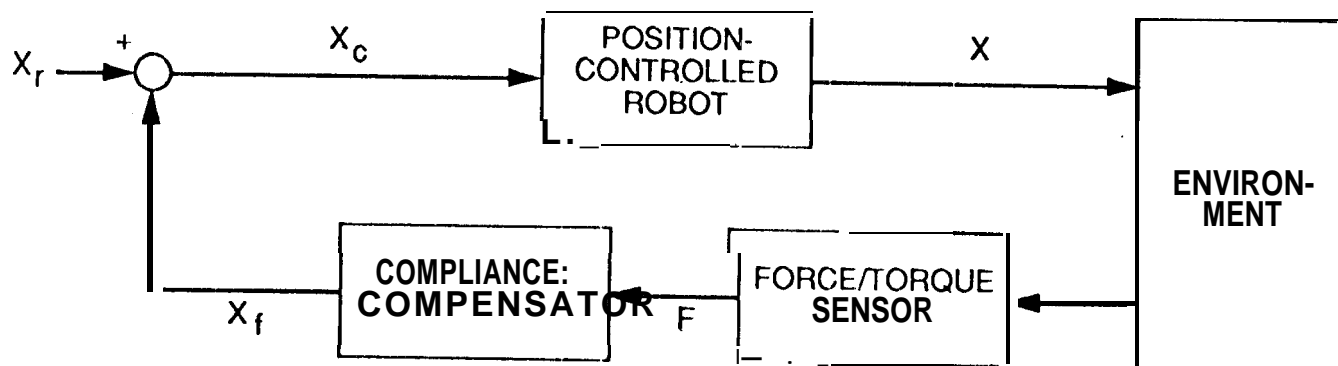


Figure 2. Position-based implicit force control system

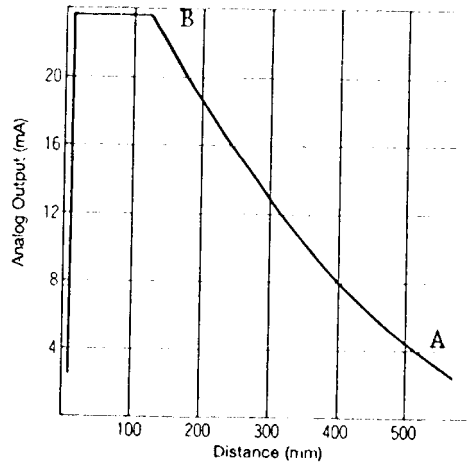


Figure 3. Characteristics of the proximity sensor

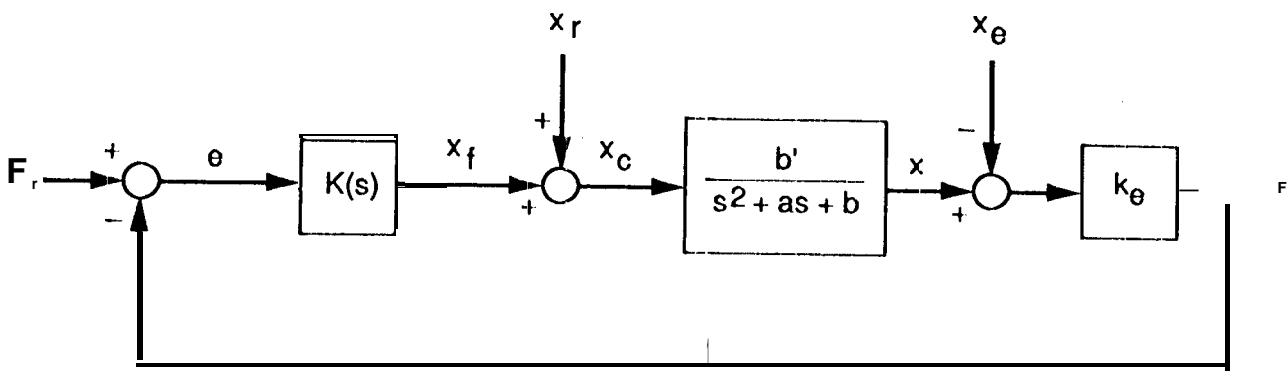


Figure 4. Admittance-based force control system

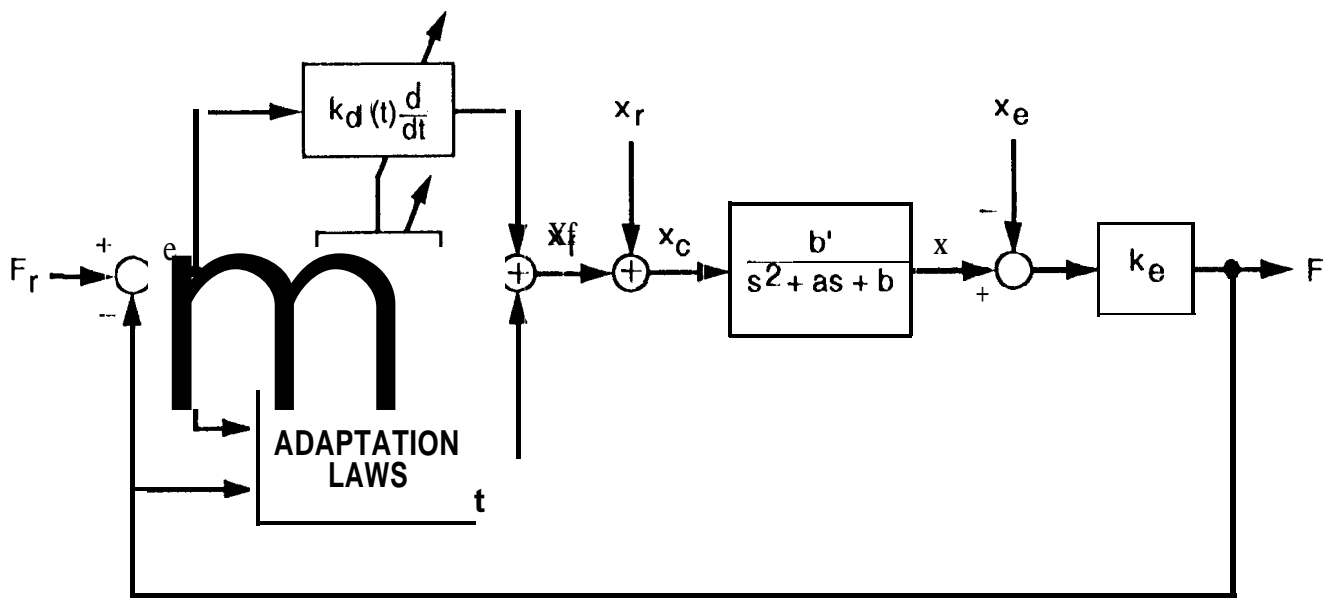


Figure 5. Adaptive PID force control scheme

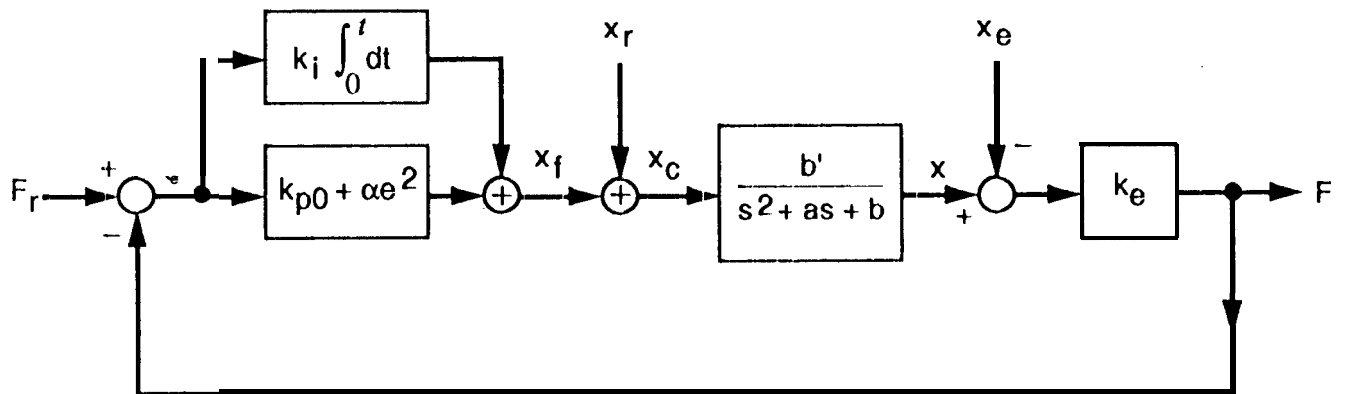


Figure 6. Adaptive PI force control scheme

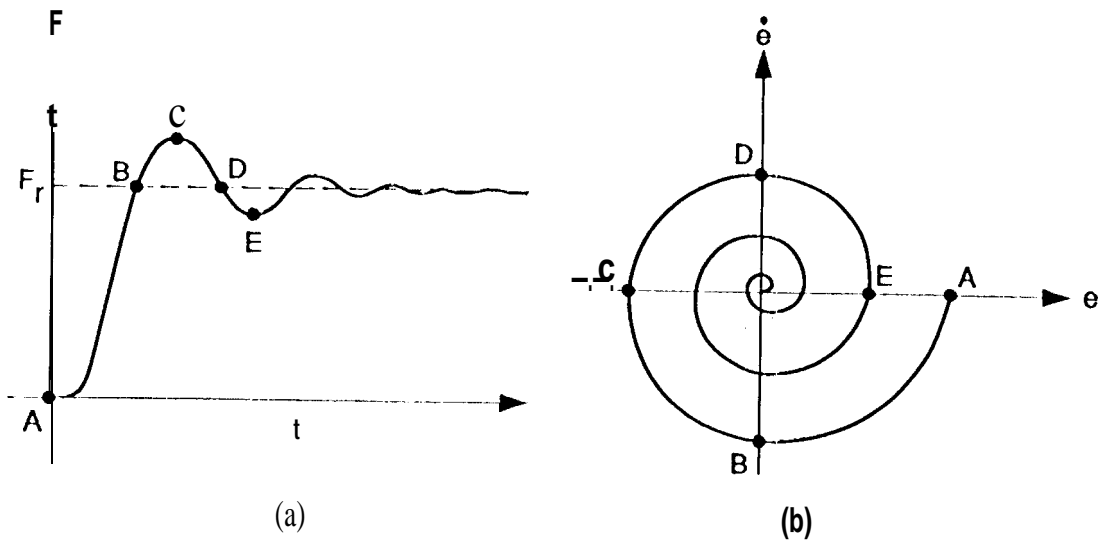


Figure 7. Typical force response and phase plot

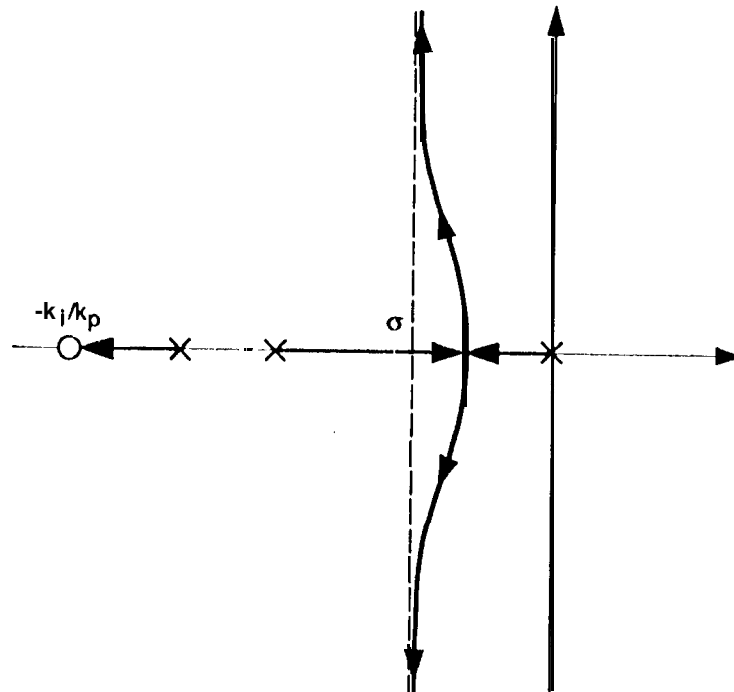


Figure 8. Root locus plot for PI force compensator

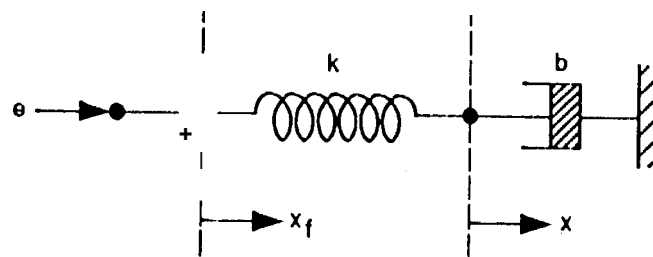


Figure 9. Mechanical realization of PI force compensator

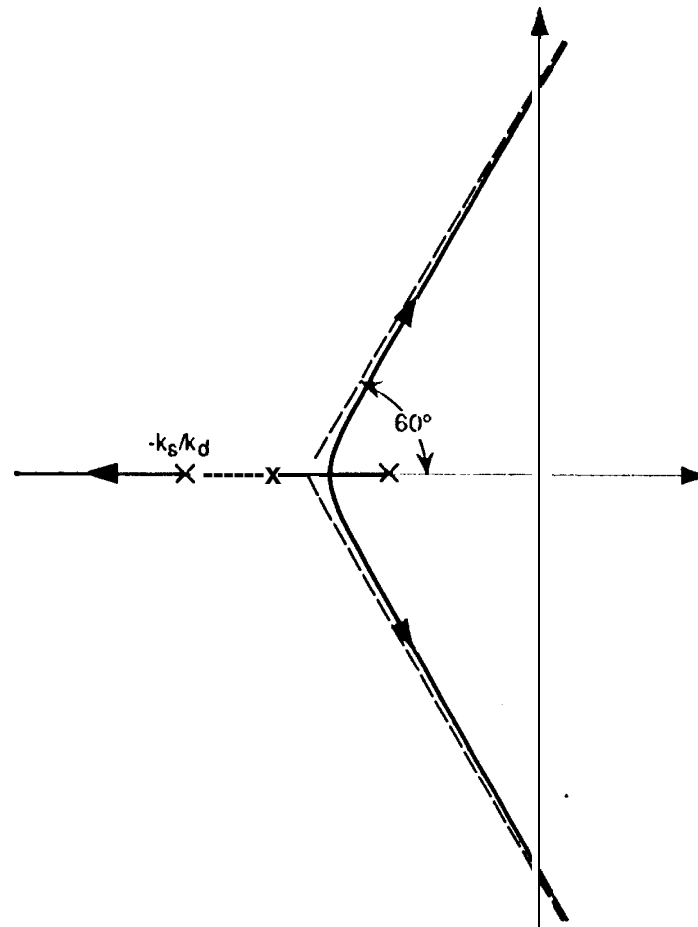


Figure 10. Root locus plot for conventional compliance compensator

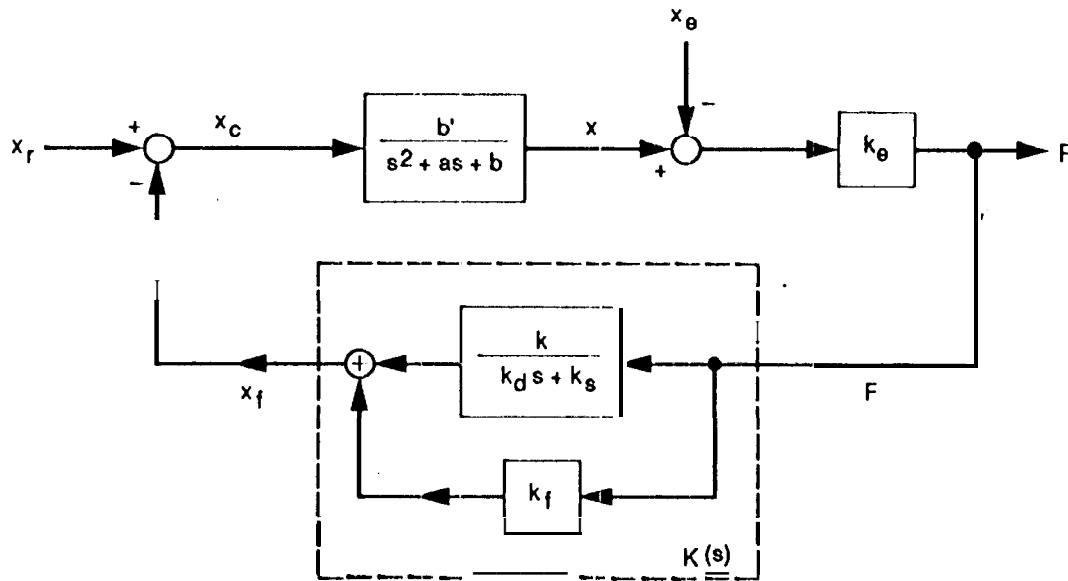


Figure 11. Lag-pius-feedforward compliance control scheme

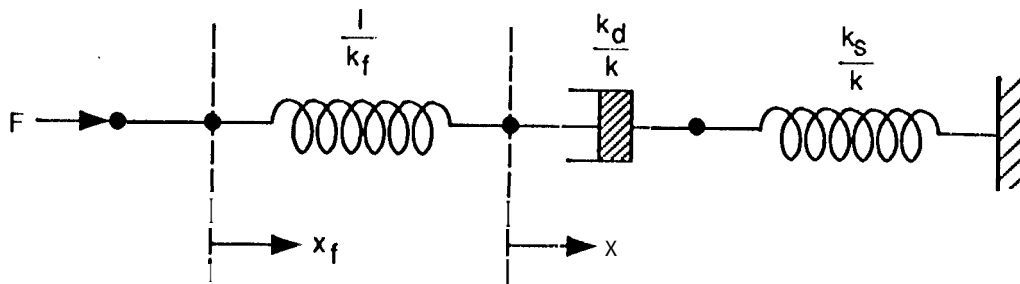


Figure 12. Mechanical realization of lag-plus-feedforward compliance compensator

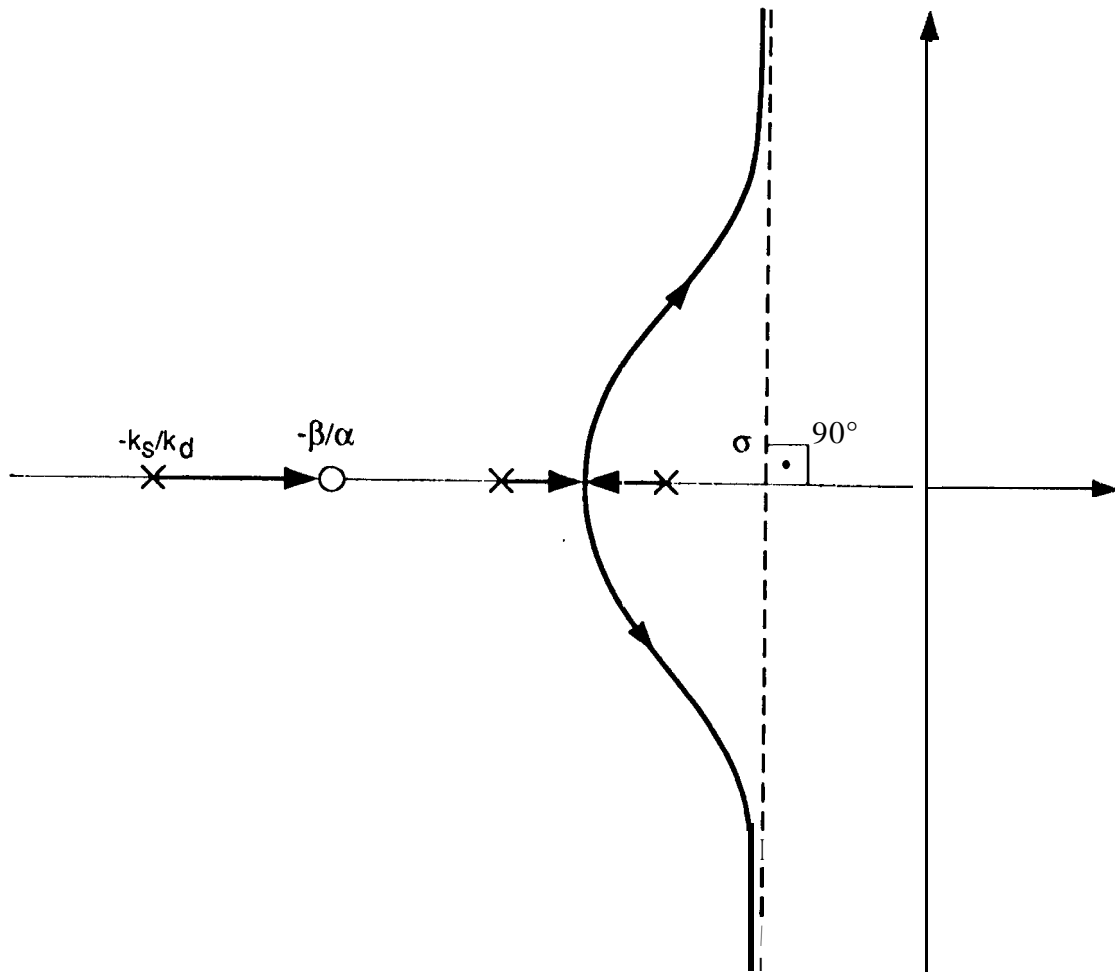


Figure 13. Root locus plot for proposed compliance compensator

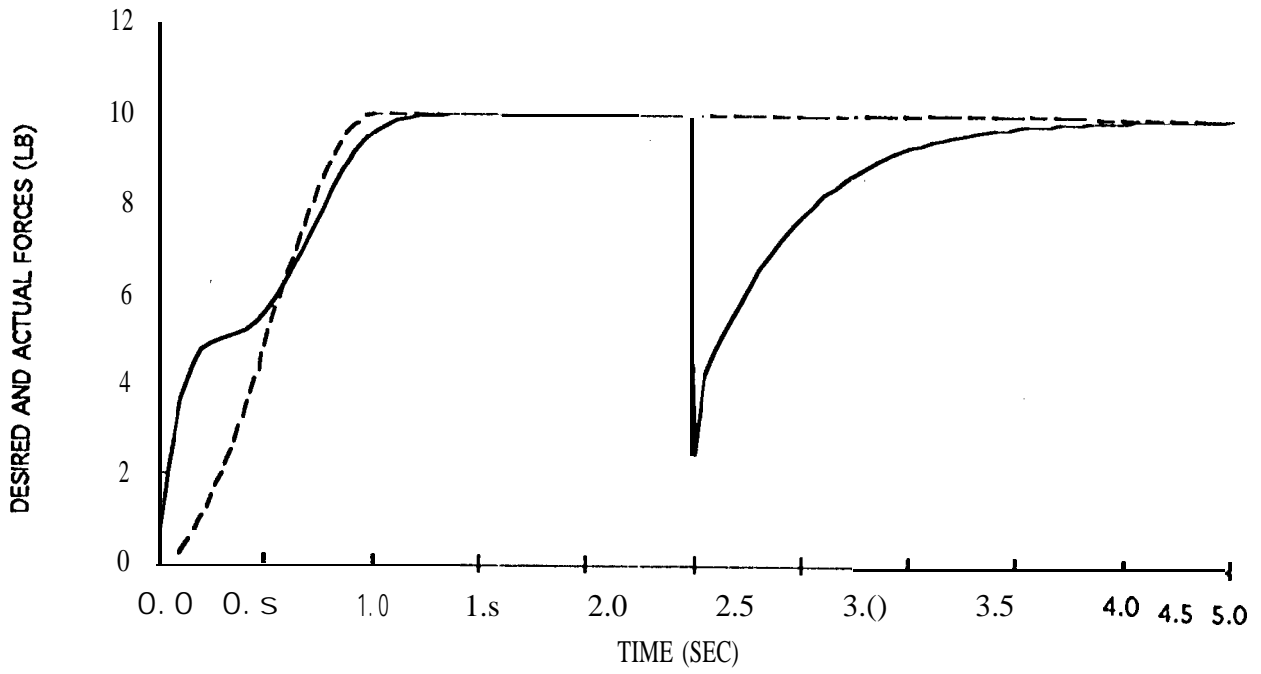


Figure 16a. Variation of the contact force F in the simulation study

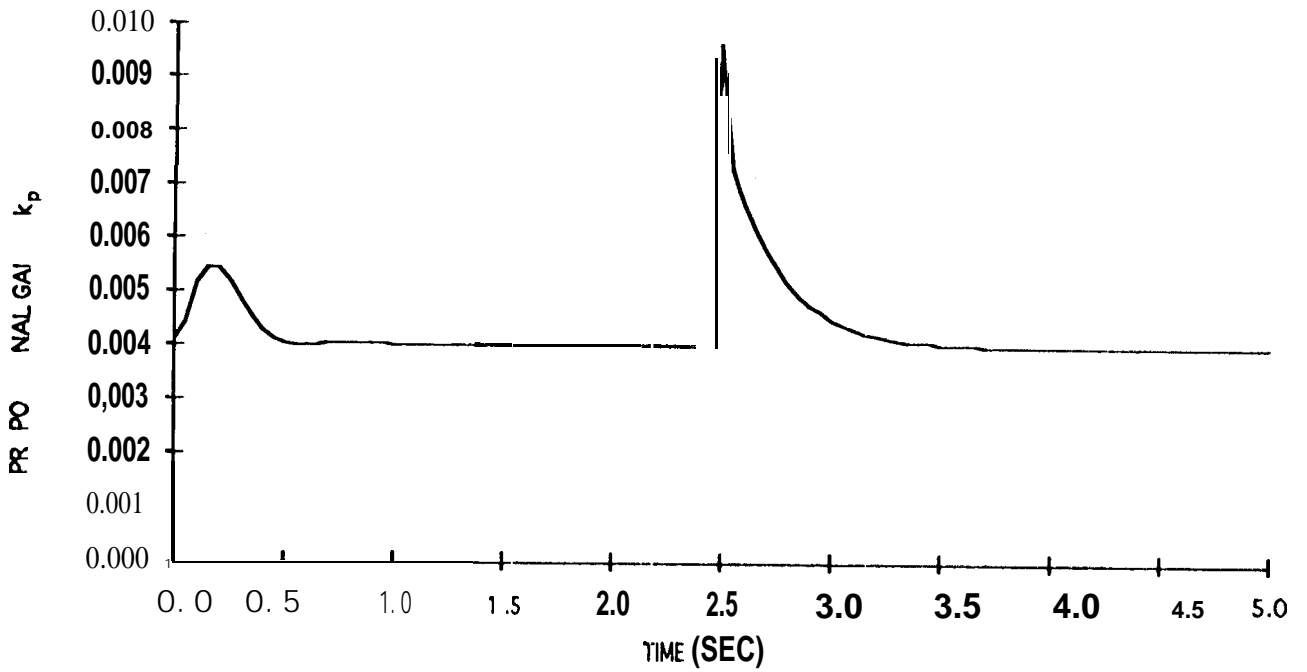


Figure 16b. Variation of the adaptive proportional gain k_p in the simulation study

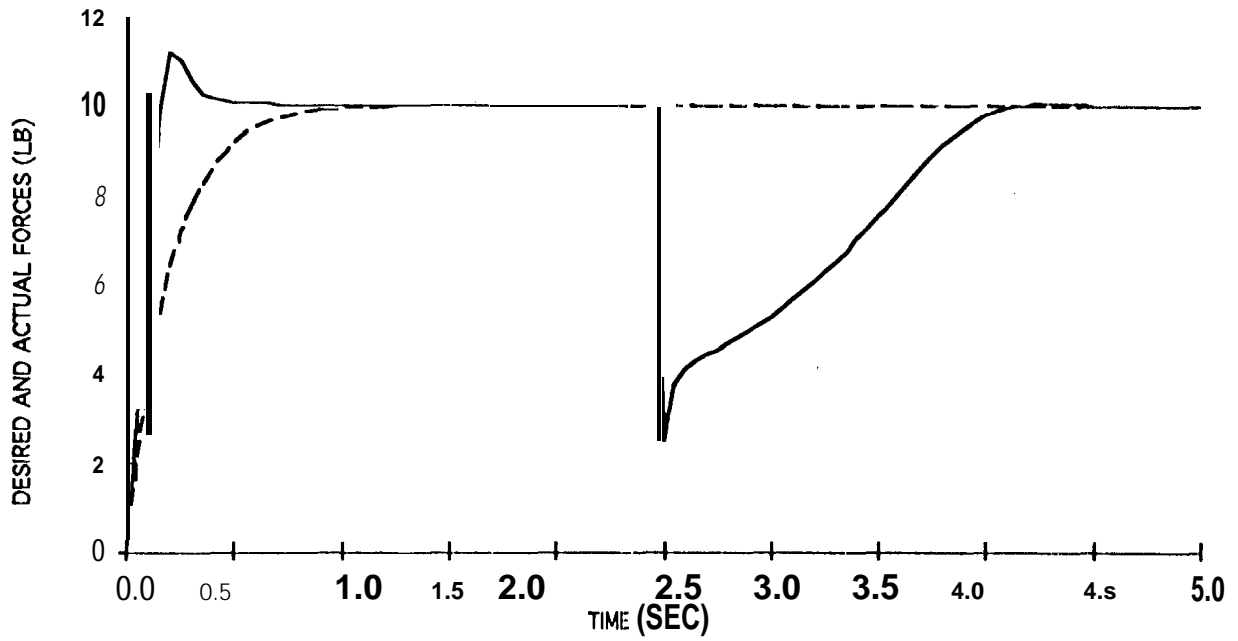


Figure 17a. Variation of the contact force F in the simulation study

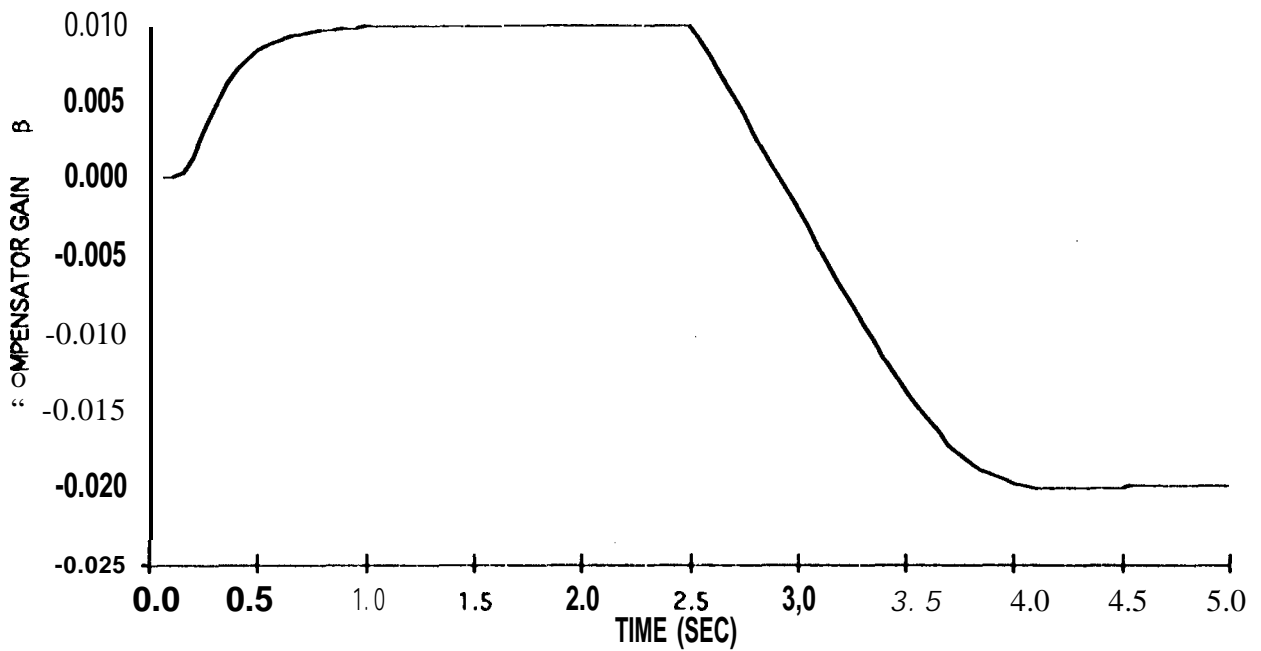


Figure 17b. Variation of the adaptive compensator gain β in the simulation study